Sofie Toska Halvorsen

Effect of Hunga Tonga–Hunga Ha'apai eruption on tidal winds and temperature of the MLT

Master's thesis in MTFYMA
Supervisor: Patrick Joseph Espy
Co-supervisor: Yvan Orsolini
June 2024

Master's thesis

NTNU
Norwegian University of Science and Technology
Faculty of Natural Sciences
Department of Physics

NTNU
Norwegian University of
Science and Technology

Sofie Toska Halvorsen

Effect of Hunga Tonga–Hunga Ha'apai eruption on tidal winds and temperature of the MLT

Master's thesis in MTFYMA
Supervisor: Patrick Joseph Espy
Co-supervisor: Yvan Orsolini
June 2024

Norwegian University of Science and Technology
Faculty of Natural Sciences
Department of Physics

NTNU
Norwegian University of
Science and Technology

Sofie Toska Halvorsen

Effect of Hunga Tonga–Hunga Ha'apai eruption on tidal winds and temperature of the MLT

Master's thesis in Physics and Mathematics
Supervisor: Patrick Joseph Espy
Co-supervisor: Yvan Orsolini
June 2024

Norwegian University of Science and Technology
Faculty of Natural Sciences
Department of Physics

NTNU

ABSTRACT

This master's thesis investigates the impact of the Hunga Tonga-Hunga Ha'apai volcanic eruption on the dynamics of the Mesosphere and Lower Thermosphere (MLT). Utilizing data from SKiYMET radar systems at Rothera and Trondheim, the study analyzes wind pattern anomalies and tidal amplitudes post-eruption. While the results indicate potential influences on the 16-day planetary wave, definitive conclusions regarding the eruption's effects remain elusive due to the need for further analysis, including the potential impact of stratospheric warming. This research provides the foundation for future studies aimed at understanding volcanic eruptions' long-term effects on atmospheric dynamics and improving climate models and predictions.

SAMMENDRAG

Denne masteroppgaven undersøker effekten av Hunga Tonga-Hunga Ha'apai vulkanutbruddet på dynamikken i mesosfæren og nedre termosfære (MLT). Ved bruk av data fra SKiYMET radarsystemer ved Rothera og Trondheim analyserer studien avvik i vindmønstre og tidevannsamplituder etter utbruddet. Resultatene indikerer mulige påvirkninger på den 16-dagers planetbølgen, men definitive konklusjoner om utbruddets effekter forblir usikre på grunn av behovet for videre analyse, inkludert den potensielle påvirkningen av stratosfæriske varminger. Denne forskningen legger grunnlaget for fremtidige studier rettet mot å forstå vulkanutbrudds langsiktige effekter på atmosfæredynamikk og forbedre klimamodeller og -prediksjoner.

PREFACE

This master's thesis represents the culmination of the five-year Applied Physics and Mathematics program at the Norwegian University of Science and Technology (NTNU), carrying a weight of 30 ECTS credits. The research was conducted within the Department of Physics under the supervision of Prof. Patrick Joseph Espy and Prof. Yvan Orsolini.

I would like to express my sincere gratitude to Patrick Espy and Yvan Orsolini for their support and guidance throughout this exciting project. Their mentorship has been invaluable during weekly meetings during both the specialization project and the master's thesis. I am grateful for the opportunity to explore the effects of such a recent and impactful event, which has provided me with a wealth of new knowledge and insights.

I would also like to extend my thanks to Ane Dyrkorn for being a valuable discussion partner and friend throughout this past year. Having someone at a similar academic level to discuss and analyze various aspects of this thesis has been an invaluable asset. Through our different tasks related to the Hunga Tonga-Hunga Ha'apai eruption, I have gained a deeper understanding of the event on multiple levels.

The specialization project (TFY4510) were written on a similar topic, and this thesis will therefore bear similarities to the project report delivered in December 2023.

CONTENTS

LIST OF FIGURES

LIST OF TABLES

ABBREVIATIONS

List of all abbreviations in alphabetic order:

- **NTNU** Norwegian University of Science and Technology
- **MLT** Mesosphere and Lower Thermosphere
- **SSW** Sudden Stratospheric Warming
- **SFW** Stratospheric Final Warming
- **MAD** Median Absolute Deviation
- **SH** Southern Hemisphere
- **NH** Northern Hemisphere

CHAPTER

ONE

INTRODUCTION

1.1 Motivation

The Earth's climate and weather patterns are greatly influenced by the Sun's energy, which leads to significant changes in energy throughout the day and year. These changes occur on different timescales and across various parts of the world. A specific layer in the atmosphere, known as the Mesosphere and Lower Thermosphere (MLT), located approximately 50 to 130 kilometers above the Earth's surface, plays a crucial role in balancing the energy received from the Sun and the movements of air in the lower atmosphere[1].

A noteworthy event that had significant implications for the MLT region was the eruption of the Hunga Tonga–Hunga Ha'apai volcano on January 15, 2022. This volcanic eruption released an extraordinary amount of water vapor and other substances into the atmosphere, reaching up to the mesosphere[2]. These substances alter the distribution of energy in the atmosphere, particularly influencing atmospheric tides, which are primarily driven by the Sun's energy absorbed by water vapor and ozone. These tides are critical in maintaining atmospheric balance and have a pronounced impact on wind patterns as they propagate upwards[3].

This master thesis aims to investigate the impact of the Hunga Tonga–Hunga Ha'apai eruption on the winds in the MLT region, specifically focusing on the altitudes between 80 and 100 kilometers. Utilizing data from two meteor radar systems: one located in Trondheim at Dragvoll and another at Rothera Research Station in Antarctica. By comparing the wind patterns observed during and after the eruption with historical data collected since 2012, the goal is to identify any significant changes attributable to the volcanic event.

Understanding these changes is vital for comprehending how sudden atmospheric disturbances can affect the delicate balance of the MLT region. Additionally, this research contributes to the broader field of atmospheric science by providing insights into how volcanic eruptions can influence atmospheric dynamics at high altitudes[2, 3, 4].

CHAPTER

TWO

THEORY

In this chapter, there are similarities with the project report written in the fall of 2023 for the specialization project (TFY4510).

2.1 The Earth's Atmosphere and the MLT

The Earth's atmosphere is a complex and dynamic system, composed of different layers, each with unique physical properties and phenomena. It is beneficial to have an understanding of these layers when studying events affecting the atmosphere.

2.1.1 Layers of the Atmosphere

Based on the references [1] and [5], this section explains the Earth's atmosphere, which is typically divided into several layers according to the variations in temperature with altitude. The troposphere, stratosphere, and mesosphere, significant for meteorological phenomena, are illustrated in Figure 2.1.1.

- **Troposphere:** The troposphere extends from the ground up to about 15 km in altitude, where the temperature generally decreases with height. This layer is bounded above by the tropopause and is also referred to as the lower atmosphere. It is in the troposphere that most weather phenomena occur, including cyclones, fronts, hurricanes, rain, snow, thunder, and lightning.

- **Stratosphere:** Above the tropopause lies the stratosphere, which extends up to about 50 km altitude. Here, unlike in the troposphere, the temperature increases with altitude. This layer is bounded above by the stratopause. A notable feature of the stratosphere is the concentration of ozone molecules, which play a critical role in absorbing ultraviolet radiation from the Sun.

- **Mesosphere:** Extending from the stratopause to about 85–90 km altitude is the mesosphere. In this layer, the temperature falls again with altitude, and it is bounded above by the mesopause. Above the mesopause lies the thermosphere, where the temperature rises with altitude again. The stratosphere and mesosphere together are known as the middle atmosphere.

- **Thermosphere:** Extending from the mesosphere up to 600 km, this layer experiences a significant increase in temperature with altitude. It is the layer where the auroras occur and is characterized by a low density of particles that can reach extremely high temperatures. The lower part of the thermosphere overlaps with the upper part of the mesosphere, forming the Mesosphere and Lower Thermosphere (MLT) region.

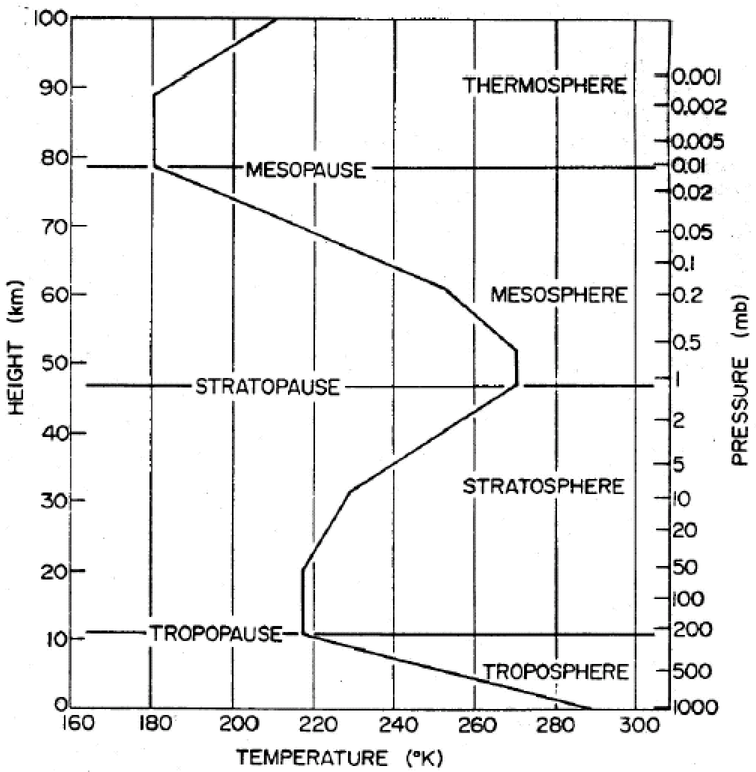

Figure 2.1.1: Layers of the atmosphere[6]

2.1.1.1 The Mesosphere and Lower Thermosphere (MLT)

The MLT region, spanning approximately from 50 to 130 km, is of particular interest in atmospheric science due to its dynamic nature and the unique phenomena occurring within it:

- **Composition and Temperature:** The MLT, particularly between 60 and 110 km, is dominated by the effects of atmospheric waves including planetary waves, tides, and gravity waves. The mesopause, at the boundary between the mesosphere and thermosphere, is characterized by temperatures low enough (around 130K) to allow for the formation of ice particles, leading to phenomena such as noctilucent clouds [7].

- **Meteorological Phenomena:** Tidal oscillations in winds and temperatures are prominent features of the MLT, with periods of 24 (diurnal) or 12 hours (semidiurnal) being dominant. These tides can be classified as either migrating (sun synchronous) or non-migrating (sun asynchronous), exhibiting different movement patterns relative to the sun [7].

- **Impact of Geophysical Events:** The MLT region is significantly affected by events such as sudden stratospheric warmings (SSWs), which are large-scale disruptions of the wind and temperature fields in the wintertime polar stratosphere. These events can be major or minor and lead to notable changes in the MLT dynamics [7].

The study of the MLT region, particularly in the context of external perturbations like volcanic eruptions, is essential for understanding the complex interactions within the Earth's atmosphere and the broader implications for global climatology and atmospheric science. The dynamics of the MLT are largely influenced by small-scale gravity waves, which play a crucial role in shaping the middle atmosphere[7].

2.1.2 Dynamics of Atmospheric Winds and Tidal Phenomena

In atmospheric science, the primary wind patterns are shaped by the interaction of heat patterns and the Earth's rotation, known as the Coriolis effect. These systems are further modulated by a variety of atmospheric waves originating from different layers such as the surface, troposphere, and stratosphere. As these waves ascend, they carry momentum and energy, influencing objects in their path. The relationship between altitude and atmospheric density is inversely proportional, leading to an increase in wave amplitude as the energy $E = mgh$ of these waves remains constant. Over time, these waves reach a breaking point where they release their accumulated momentum and energy. The periodic nature of these waves categorizes them into three primary types: atmospheric gravity waves, tidal waves, and planetary waves.

Atmospheric tidal phenomena are essentially periodic movements within the Earth's atmosphere, primarily driven by solar radiation. Key absorbers of this radiation include ozone in the stratosphere, water vapor in the troposphere, and oxygen molecules in the thermosphere, all contributing to atmospheric warming. This warming effect manifests as tidal winds, notable for their significant impact on atmospheric pressure and wind patterns, particularly in the middle atmosphere layers such as the stratosphere, mesosphere, and thermosphere. These tidal winds exhibit a daily cycle of fluctuating pressure across continental expanses. An illustration of the different Fourier components of the wind produced by heating is provided in Figure 2.1.2.

The mechanism of tidal wind generation involves solar heating of specific atmospheric regions. This heating causes expansion and subsequent creation of pressure gradients, directing winds from warmer to cooler regions. As the Earth rotates, these heated regions follow the sun's path, generating eastward-propagating waves. Besides the predominant 24-hour cycle, atmospheric tides also exhibit 12-hour and 8-hour cycles, with their prominence varying across different latitudes. The mathematical representation of these tidal components employs Fourier decomposition, under the premise that solar heating is not uniform but rather exhibits a half-cycle during the day and nullifies at night [8].

$$J(t) = \sum_{n=0}^{N} A_n(\theta, z, \lambda) \sin(n\Omega t - \phi_n(\theta, z)) \tag{2.1}$$

In Equation 2.1, Ω signifies $\frac{2\pi}{24}$ (reflecting the 24-hour cycle), with t in hours. The parameters A_n and ϕ_n denote the amplitude and phase of tidal heating, respectively, while z, θ, and λ represent height, latitude, and longitude. The term n differentiates between diurnal ($n = 1$), semidiurnal ($n = 2$), and terdiurnal ($n = 3$) atmospheric wave components, which play a crucial role in the context of this study.

Considering the fluid nature of air over the Earth's solid surface, its movement has a three-dimensional quality. Air moving northward from a heated area eventually converges with air moving southward from the opposite side, leading to a multitude of harmonics with diverse spatial and temporal wavelengths.

It's worth noting that stratospheric ozone, tropospheric water vapor, and thermospheric oxygen molecules not only absorb solar radiation but also initiate wave motions. These waves interact, forming vertical interference patterns and structures due to the interplay of higher harmonics. Consequently, diurnal waves diminish in regions distant from the equator, while semidiurnal waves intensify at higher latitudes.

Atmospheric tidal waves are characterized by their wavenumbers, with wavenumber 1 representing non-migrating waves and wavenumber 2 indicating migrating waves, along with higher wavenumbers. Migrating waves move longitudinally at the sun's pace, producing two peaks and valleys in a 24-hour period at any given longitude, constituting a 12-hour wave. Conversely, non-migrating semidiurnal tides circle the Earth at twice the sun's speed, resulting in a similar 12-hour wave. These wave types interact positively and negatively at various longitudes, posing challenges in single-station measurements like this [8].

Planetary waves (PWs) emerge from fundamental forces like Coriolis effects, driven by instabilities in moving air masses due to temperature differentials. These global-scale waves are especially pronounced in the stratosphere and, despite their typically lower amplitude compared to atmospheric tidal waves, play a crucial role in mesosphere and lower thermosphere (MLT) dynamics. The quasi-16-day wave is an example of a planetary wave (PW) with a periodicity of approximately 16 days.

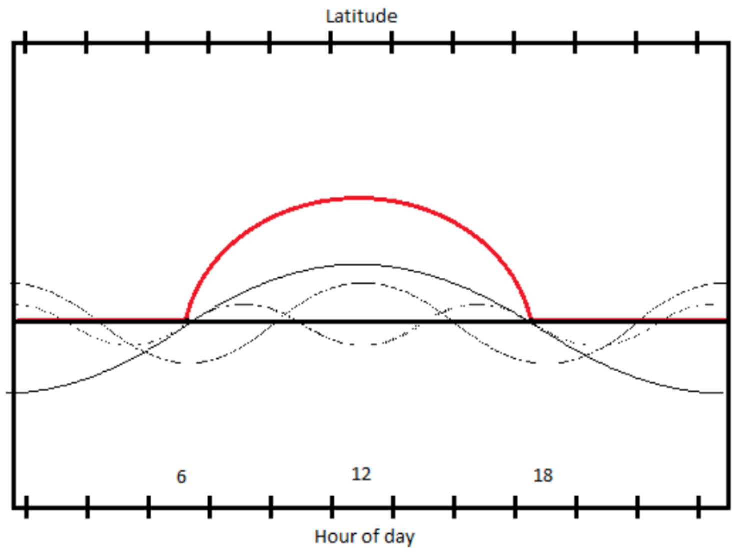

Figure 2.1.2: Illustration of the different Fourier components of the wind (black) produced by heating (red)[9].

2.2 Earth's Hemispheres

One can divide the earth into hemispheres. The hemisphere north of the equator is called the northern hemisphere, while the hemisphere south of the equator is called the southern hemisphere. These have some differences in properties.

The phenomenon of opposite seasons in the Northern and Southern Hemispheres is primarily due to the tilt of Earth's axis. Earth is tilted at an angle of approximately 23.5 degrees relative to its orbital plane around the Sun. This tilt causes different parts of the Earth to receive varying amounts of solar radiation throughout the year. During the Northern Hemisphere's summer (approximately June to September), the North Pole is tilted toward the Sun, resulting in longer days and more direct sunlight. This leads to warmer temperatures and summer conditions. Conversely, the South Pole is tilted away from the Sun, resulting in shorter days, less direct sunlight, and winter conditions in the Southern Hemisphere.The situation reverses during the Northern Hemisphere's winter (approximately December to March). The South Pole is then tilted toward the Sun, experiencing summer, while the North Pole is tilted away, leading to winter in the Northern Hemisphere. This axial tilt and the resulting variation in sunlight are responsible for the seasonal changes experienced on Earth[10].

Seasonal changes also play a crucial role in the hemispheric differences. In the Northern Hemisphere, seasons are characterized by more extreme temperature variations due to the larger land areas. Conversely, the Southern Hemisphere experiences more moderate seasonal changes because of the vast oceanic influence, which has a higher heat capacity and thus moderates temperature extremes[11].

Wind patterns in the MLT region are also influenced by the Brewer-Dobson circulation, which is stronger in the Northern Hemisphere due to the higher topographic variations and the presence of significant mountain ranges such as the Himalayas and the Rockies. This leads to more dynamic atmospheric activity and greater variation in wind speeds and directions[12].

CHAPTER

THREE

INSTRUMENTS

3.1 Rothera SKiYMET Radar

The SKiYMET radar at Rothera Research Station, located on Adelaide Island off the Antarctic Peninsula (68°S, 68°W), is a critical tool for meteorological research in the mesosphere and lower thermosphere (MLT). This advanced radar system employs a 6 kW peak power solid-state transmitter, broadcasting at a frequency of 32.5 MHz with a pulse repetition frequency of 2144 Hz. The radar's antenna array is configured as an interferometer with five elements, enabling precise measurements of meteor echo positions and velocities through Doppler shift analysis. These capabilities allow the radar to measure horizontal winds by tracking the movement of meteors at altitudes between approximately 75 and 105 kilometers. Additionally, it assesses atmospheric temperatures through the decay rates of meteor echoes and calculates meteor flux by analyzing data from several thousand meteors daily. This robust setup makes the SKiYMET radar exceptionally effective for monitoring atmospheric conditions and capturing high-resolution data on atmospheric tides within a vertical range of 79–101 km, providing invaluable insights into the dynamics of the MLT region[13].

3.2 Trondheim SkiYMET Radar

This section relies on findings from [14] and [15]. The SKiYMET meteor radar used for data representing the northern hemisphere, is located at Dragvoll, Trondheim (63.4°N,10.5°E). This instrument is equipped with eight transmitters and five receivers for studying ionized meteor trails in the Earth's atmosphere. These trails, lasting up to four seconds and influenced by atmospheric winds, are analyzed for velocity, distance from the radar, azimuth and zenith angles, and ambiguity.

The radar operates at approximately 1 kHz (transmission) and 34.21 MHz (reception) frequencies with a wavelength of $\lambda \approx 9$ m. The antennas are configured octagonally to optimize radiation focus between zenith angles of 10° to 90° and to create specific interference patterns at azimuth angles, especially at multiples of 45°.

The receiving antennas are positioned in a cross formation with a central antenna and four others at 90° intervals. Two antennas are placed at $r = 2\lambda$ from the center, aiding in determining meteor positions by analyzing phase differences, with the aim of selecting the position with minimal error below a preset threshold. Ambiguities are noted when meteors exhibit similar minimum error values.

Meteor detection rates average around 15,000 per day, influenced by the Earth's rotation and orbit, with variations due to the Earth's axial tilt affecting seasonal detection rates. In Figure 3.2.1 there is an overview of the radar location and setup at Dragvoll.

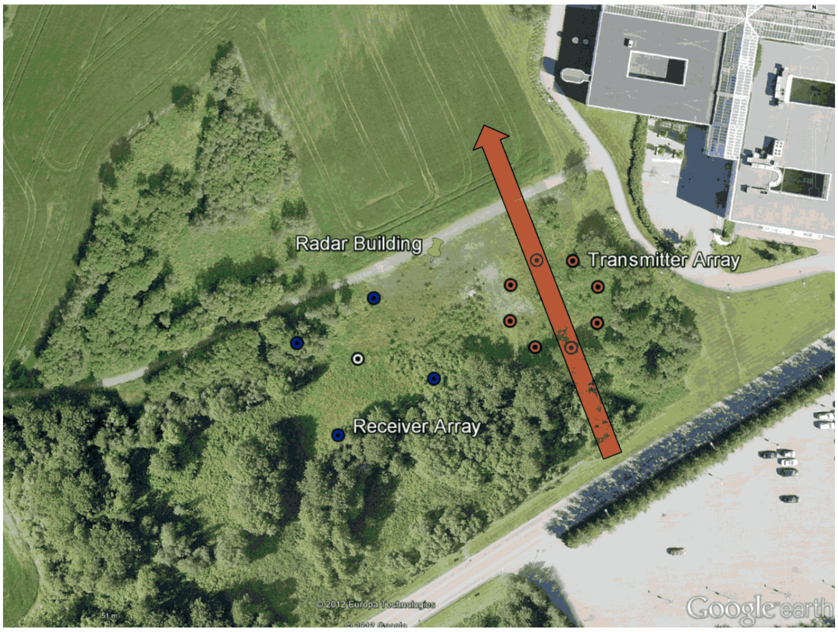

Figure 3.2.1: Overview of the setup of the SKiYMET radar at Dragvoll, Trondheim [15].

The SKiYMET radar employs digitization techniques and computer methods, allowing for real-time data processing, detection, and analysis of meteor occurrences. This enables the determination of meteor trajectories, radial drift speeds, decay times, and atmospheric parameters such as wind, temperature, and diffusion coefficients. The system's design incorporates modern interferometric techniques with wider beams, enhancing the detection and analysis capabilities across the entire sky.

Real-time data streaming and analysis are facilitated by a software system running on UNIX-based platforms. This system efficiently manages data acquisition, echo detection, and subsequent processing, ensuring high accuracy and minimal data loss. The radar's software algorithms are adept at distinguishing meteor echoes from other atmospheric phenomena, enhancing the reliability of the collected data.

3.3 Data from the SKiYMET radar

Figure 3.3.1, is an example of how the data from the SKiYMET radar in Trondheim can be viewed directly from the atmospheric group's webpage [16]. It displays graphics of the zonal and meridional wind.

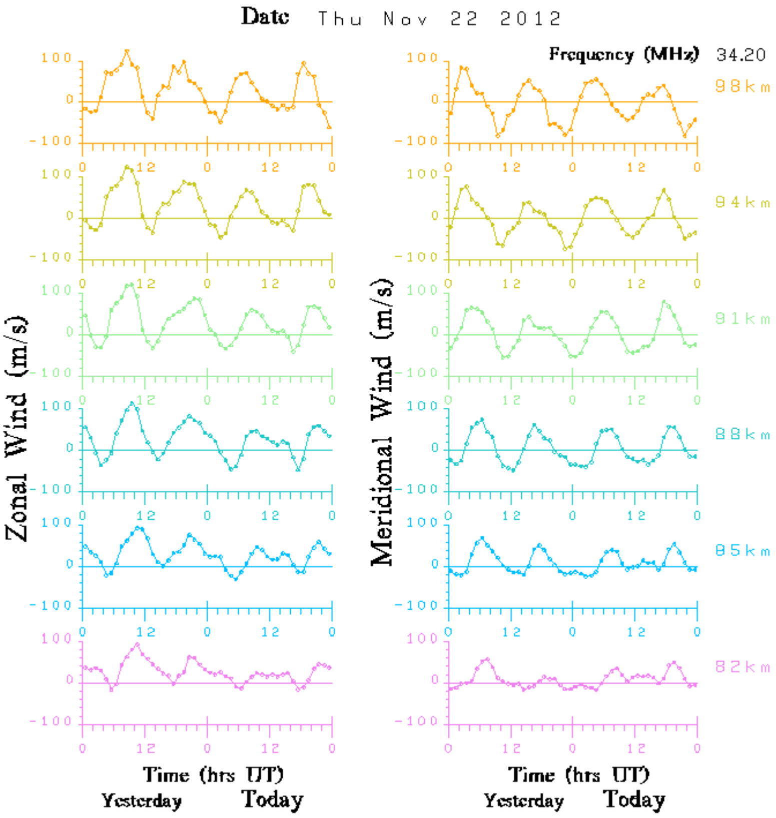

Figure 3.3.1: Wind data from the SKiYMET meteor radar available at the Atmospheric Physics group webpage[16].

The data files obtained from the radar in Trondheim are presented in Figure 3.3.2, and the files obtained from the radar located at Rothera are identical. These files are foundational to the methodology used in this study, as the whole study builds on these files, where there is one file for each day.

jupyter hw20220128.trondheim.hwd✔ 29.01.2022 Logout

File Edit View Language Plain Text

```
 FINAL ESTIMATES for 2022/01/28
k, ht =  1  82.
times    .5  1.5  2.5  3.5  4.5  5.5  6.5  7.5  8.5  9.5 10.5 11.5 12.5 13.5 14.5 15.5 16.5 17.5 18.5 19.5 20.5 21.5 22.5 23.5
zonal    58   44   29    5    1  -18  -27  -20   18   41   48   43   41   46   46   29   15    8   -5  -11    2    1    6   21
merid   -18  -32  -26  -34  -23   -9    7   27   30   11    4  -15  -14   -7    1    8   20   38   39   35   23   15   29   32
# pts    84   84  100   93   96   64   60   39   42   39   42   38   39   48   58   50   62   67   64   63   74   86   86   75
k, ht =  2  85.
times    .5  1.5  2.5  3.5  4.5  5.5  6.5  7.5  8.5  9.5 10.5 11.5 12.5 13.5 14.5 15.5 16.5 17.5 18.5 19.5 20.5 21.5 22.5 23.5
zonal    59   29   12  -14  -30  -42  -23    3   39   55   51   42   31   35   31  -16  -15  -15  -12  -18   -7    7   25   47
merid   -41  -51  -47  -48  -14   18   46   58   33   -3  -10  -18  -20   -6    2   28   32   42   41   36   37   45   50   30
# pts    89  127  120  113  106   97   80   53   62   69   56   55   52   60   58   47   66   68   64   66   83  105  115   98
k, ht =  3  88.
times    .5  1.5  2.5  3.5  4.5  5.5  6.5  7.5  8.5  9.5 10.5 11.5 12.5 13.5 14.5 15.5 16.5 17.5 18.5 19.5 20.5 21.5 22.5 23.5
zonal    47   24   -9  -37  -31  -25   19   54   76   78   54   40   16   14  -11  -36  -22  -18  -22   -9    8   40   62   42
merid   -57  -62  -50  -13   10   41   66   53   21    0  -22  -25  -15   11   14   35   45   45   40   49   62   44   18  -18
# pts   123  152  150  116  101   97  115   84   73   80   83   95   81   74   64   53   65   74   83   89  100  101   99   76
k, ht =  4  91.
times    .5  1.5  2.5  3.5  4.5  5.5  6.5  7.5  8.5  9.5 10.5 11.5 12.5 13.5 14.5 15.5 16.5 17.5 18.5 19.5 20.5 21.5 22.5 23.5
zonal   -11  -16  -43  -26   -9   24   58   80   88   77   50   13   -7  -22  -39  -41  -12  -14  -15   19   46   59   55  -17
merid   -43  -42    6   40   57   62   47   16   -6  -16  -24  -10    2   19   22   31   60   57   56   67   53    7  -14  -60
# pts   112  116  116  125  129  127  150  103   81  103   75   65   75   51   48   52   57   72   73   80   87   62   41   37
k, ht =  5  94.
times    .5  1.5  2.5  3.5  4.5  5.5  6.5  7.5  8.5  9.5 10.5 11.5 12.5 13.5 14.5 15.5 16.5 17.5 18.5 19.5 20.5 21.5 22.5 23.5
zonal   -53  -44  -26    6   41   60   81   80   75   56   27  -10  -28  -31  -31   -9   18    7   14   44   61   53   -2  -61
merid     4   15   32   53   64   54   30    5  -13  -19  -16    3    8    4    8   11   52   55   66   57    1  -53  -80  -47
# pts    69   90   87  101  140  157  129   85   81   85   42   39   53   46   27   34   33   34   55   58   41   37   30   41
k, ht =  6  98.
times    .5  1.5  2.5  3.5  4.5  5.5  6.5  7.5  8.5  9.5 10.5 11.5 12.5 13.5 14.5 15.5 16.5 17.5 18.5 19.5 20.5 21.5 22.5 23.5
zonal   -47  -21   26   55   65   67   83   65   65   33   12    7  -11  -14  -22   21   30   15   63   81   40  -41  -91  -58
merid     8   19   24   46   61   44   24   11   -9   -7   -7    1    4    5   11   11   29   41   50   46  -36 -106  -19  -35
# pts    33   35   39   53   75   86   55   39   42   31   21   21   27   17   12   11   11   10   11   17   14    9   14   16
k, ht =  7  103.
times    .5  1.5  2.5  3.5  4.5  5.5  6.5  7.5  8.5  9.5 10.5 11.5 12.5 13.5 14.5 15.5 16.5 17.5 18.5 19.5 20.5 21.5 22.5 23.5
zonal   999  999  999  999  999  999  999  999  999  999  999  999  999  999  999  999  999  999  999  999  999  999  999  999
merid   999  999  999  999  999  999  999  999  999  999  999  999  999  999  999  999  999  999  999  999  999  999  999  999
# pts     0    0    0    0    0    0    0    0    0    0    0    0    0    0    0    0    0    0    0    0    0    0    0    0
k, ht =  8  109.
times    .5  1.5  2.5  3.5  4.5  5.5  6.5  7.5  8.5  9.5 10.5 11.5 12.5 13.5 14.5 15.5 16.5 17.5 18.5 19.5 20.5 21.5 22.5 23.5
zonal   999  999  999  999  999  999  999  999  999  999  999  999  999  999  999  999  999  999  999  999  999  999  999  999
merid   999  999  999  999  999  999  999  999  999  999  999  999  999  999  999  999  999  999  999  999  999  999  999  999
# pts     0    0    0    0    0    0    0    0    0    0    0    0    0    0    0    0    0    0    0    0    0    0    0    0
```

Figure 3.3.2: Datafile from the SKiYMET meteor radar for the date 28.01.2022.

CHAPTER

FOUR

METHODS

Due to the overlap in method in this master thesis and the project report written in the fall of 2023, there will be similarities in the methodology of the two reports.

4.1 Preparation of Data

The data preparation process involved reading the HWD data files and combining the date and time into a single datetime column within a pandas DataFrame. This datetime format facilitated more straightforward data manipulation and analysis.

Each data file contains information on the height, zonal (u) and meridional (v) wind components, and points (pts). We extracted these values and stored them in a structured DataFrame, ensuring consistency and ease of access for further analysis.

To gather data for the climatology data from the pre-eruption dates were collected, and combined with post eruption data. That way ensured that the eruption period were not included in the climatology. The pre-eruption period includes data from August 10, 2012, to October 29, 2021, while the post-eruption period spans from May 1, 2022, to December 31, 2023. Data from the eruption period (November 1, 2021, to April 30, 2022) was also separately collected and prepared.

The processing and filtering of the data were achieved using custom Python functions. These functions read the HWD data files, handled missing or erroneous values, and combined the data into a comprehensive DataFrame. The resulting DataFrame was then used to model tidal components of wind data, facilitating a detailed examination of the underlying tidal influences on wind patterns.

In particular, we employed a function to fit tidal models to the wind components (u and v) using curve fitting techniques. This approach allowed to extract amplitudes for different tidal components, providing insights into the semidiurnal variations in wind patterns.

4.2 Tidal Fit

To further understand the tidal influences on wind data, a tidal model fitting procedure were applied. This method involved fitting a predefined tidal model to the wind components over specific time windows. By doing so, the wind data was decomposed into its constituent tidal components, including 24-hour, 12-hour, 8-hour, and 48-hour cycles.

The tidal model implemented employs sine and cosine functions to represent the different waves. The model is expressed as follows:

$$\begin{aligned} f(t) = & A_0 + A_{48}\cos\left(\frac{2\pi t}{48}\right) + B_{48}\sin\left(\frac{2\pi t}{48}\right) \\ & + A_{24}\cos\left(\frac{2\pi t}{24}\right) + B_{24}\sin\left(\frac{2\pi t}{24}\right) \\ & + A_{12}\cos\left(\frac{2\pi t}{12}\right) + B_{12}\sin\left(\frac{2\pi t}{12}\right) \\ & + A_8\cos\left(\frac{2\pi t}{8}\right) + B_8\sin\left(\frac{2\pi t}{8}\right) \end{aligned} \tag{4.1}$$

where in the equation:

- t represents the time of day in hours.
- A_0 is the constant term, indicating the baseline level of the parameter being measured.
- $A_{48}, A_{24}, A_{12}, A_8$ are the amplitude coefficients for the cosine components of the 48-hour (bi-daily), 24-hour (diurnal), 12-hour (semi-diurnal), and 8-hour tidal cycles, respectively.
- $B_{48}, B_{24}, B_{12}, B_8$ are the amplitude coefficients for the sine components of the corresponding tidal cycles.
- The expressions $\frac{2\pi t}{48}, \frac{2\pi t}{24}, \frac{2\pi t}{12}, \frac{2\pi t}{8}$ denote the angular frequencies for the respective tidal components.

A distinctive aspect of this analysis is the adoption of a four-day window for model fitting, aligning with methodologies applied in similar studies. Importantly, this method follows similar techniques used by Hibbins and Jarvis in their study titled 'A long-term comparison of wind and tide measurements in the upper mesosphere recorded with an imaging Doppler interferometer and SuperDARN radar at Halley, Antarctica' [17]. Such a window is chosen to balance the need for capturing significant tidal patterns while mitigating the influence of transient atmospheric events.

4.3 Despiking Data Using the Median Absolute Deviation (MAD)

The data from Rothera included some significant spikes. To remove spikes from the dataset, the Median Absolute Deviation (MAD) were employed. MAD is defined as the median of the absolute deviations from the median of the data. This method is particularly useful for identifying outliers because it is less sensitive to extreme values compared to the standard deviation [18].

Mathematically, MAD is expressed as:

$$\text{MAD} = \text{median}(|X_i - \text{median}(X)|)$$

where X represents the data values, X_i are individual data points, and median(X) is the median of the dataset.

To identify and handle outliers, the MAD were calculated for each numeric column in the DataFrame. A threshold was set using a MAD multiplier, where values that deviated from the median by more than this threshold were considered spikes and set to NaN. The threshold is defined as:

$$\text{Threshold} = k \times \text{MAD}$$

where k is the MAD multiplier, which for the Rothera data were set to 3 and for the Trondheim data were set to 5. This means any data point with an absolute deviation greater than three/five times the MAD was marked as a spike.

As a precaution the filtering method were tested. The data from Rothera had multiple extreme spikes. This can bee seen in Figure 4.3.1a.

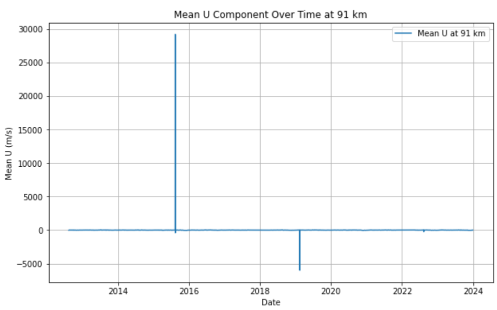

(a) The zonal mean wind at 91km before filtering

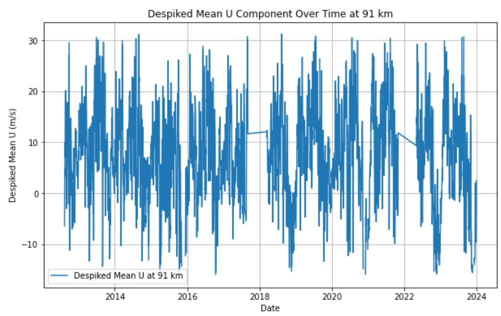

(b) Despiked data of the zonal mean wind at 91km altitude

Figure 4.3.1: Comparison of the zonal mean wind at 91km altitude before and after despiking

Figure 4.3.1 shows the data pre spike removal(Figure 4.3.1a) and post spike removal (Figure 4.3.1b. The spike removal were done for all the different components both for mean values and amplitudes for both the Rothera data and Trondheim data.

4.4 Climatology

Climatology refers to the analysis of long-term weather patterns and trends. This analysis often involves the calculation of mean values over extended periods, helping to understand the typical meteorological conditions for a given time frame or location. In this study the climatology is made using data from the time periods pre- and post-eruption period.

During the work on this thesis, it was found more advantageous to use the median to form the climatology's, instead of a climatology using the mean. This is because of the big spikes in the data. The median is less affected by outliers and extreme values that can skew the mean. It provides a more robust representation of the typical values in the dataset, reducing the influence of random noise and extreme events. The climatology is done on both the mean wind and the different amplitudes. The final plot is a contour plot with the x-axis being day from 1st of November, going from 1st of November til 30th of April, and the y-axis shoes the different altitudes going from 82km to 98km altiude. Then there is a colorbar for showing the wind values in m/s.

4.4.1 Rolling Mean

To smooth the climatology, a 30-day rolling mean method was utilized. This approach involves calculating a moving average over a 30-day period, which smooths out short-term fluctuations and highlights longer-term trends in the data. The rolling mean is particularly effective in reducing noise and making underlying patterns more apparent.

A rolling mean, also known as a moving average, is a common technique in time series analysis. It works by averaging a fixed number of sequential data points, and then moving this window along the time axis to create a new series of averaged values. In this study, a 30-day window was chosen, meaning that each point in the smoothed series represents the average of 30 consecutive days of data.

Mathematically, the rolling mean $\overline{X_t}$ at time t with a window size of N is given by:

$$\overline{X_t} = \frac{1}{N}\sum_{i=0}^{N-1} X_{t-i} \tag{4.2}$$

where X_t is the value at time t, and N is the number of periods in the rolling window, in this project it is set to 30 days[19].

Figure 4.4.1a illustrates the climatology before applying the rolling mean, showing a graph with significant daily fluctuations. In contrast, Figure 4.4.1b shows the climatology after applying the 30-day rolling mean, where the data appear much smoother and the long-term trends are more evident.

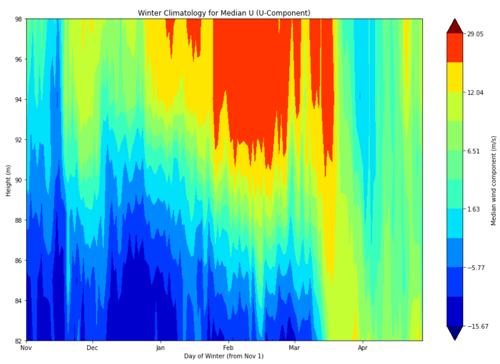

(a) Climatology before 30-day rolling mean

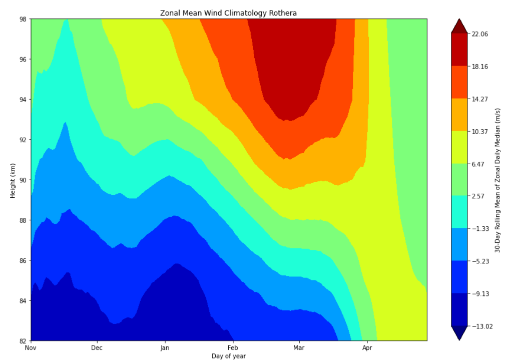

(b) Climatology after 30-day rolling mean

Figure 4.4.1: The two figures illustrates the difference between a) climatology before 30 day rolling mean and b) after 30 day rolling mean

4.5 Anomaly

To further analyze the data, this project employs a method to calculate and analyze anomalies for the mean wind components and tidal components. Using the 30-day rolling mean, anomalies are calculated by subtracting the climatological value from each data point during the eruption period. These anomalies are then plotted similarly to the climatology, with altitude on the y-axis and days from November 1st on the x-axis, but the color scale represents the anomaly values.

Analyzing these anomalies helps identify how the eruption may affect tidal winds, revealing patterns such as planetary, semi-diurnal, and diurnal waves.

4.6 Lomb-Scargle Periodogram

The process of a Lomb-Scargle Periodogram involves calculating the power spectrum by employing a least-squares fitting approach to approximate a sinusoidal model to the time-series data at each frequency of interest. This method adjusts for the gaps and irregularities in the sampling schedule, unlike the classical Fourier transform which assumes evenly spaced data points. The output from the Lomb-Scargle periodogram is a plot of the power as a function of frequency, from which the significant periodic components can be located, making it possible to pinpoint the fundamental frequencies and their harmonics in the data[20].

Key strengths of the Lomb-Scargle method include its applicability to datasets with gaps, its resilience against the uneven spacing of observations, and its ability to handle observational errors effectively. It is important to understand and mitigate the subtleties involved in its application, such as choosing appropriate frequency grids and understanding the statistical significance of detected periods, to ensure accurate interpretation of the periodogram results. [20]

4.7 Wavelet Transform

Wavelet analysis provides a method for investigating time-series data, especially when dealing with data that include gaps or irregular sampling intervals. This analysis technique utilizes wavelets—small, wave-like oscillations that are localized in both time and frequency. Unlike the Fourier transform, which requires stationary data, wavelet transforms are adaptable to the evolving frequencies and amplitudes within a dataset, making them particularly suited for environmental studies where data irregularities are common[21].

This method's flexibility in handling non-uniformly sampled data ensures that it captures the full spectrum of variability in wind behavior, providing a comprehensive tool for analysis. Thus, the adoption of wavelet analysis in this research enriches the exploration of tidal wind dynamics, offering detailed insights that are crucial for both theoretical and applied meteorological studies[21]. In this study, the wavelets lets us see how the presence of a wave differs throughout time. The wavelet function for a single sinuswave with a period of 16-days and an amplitude of 1 will look like the wavelet in Figure 4.7.1.

As the wavelets are plotted as contour plots, a plot of the extraction of the wave of interest can be plotted. This is a plot of the intensity of the wave over time.

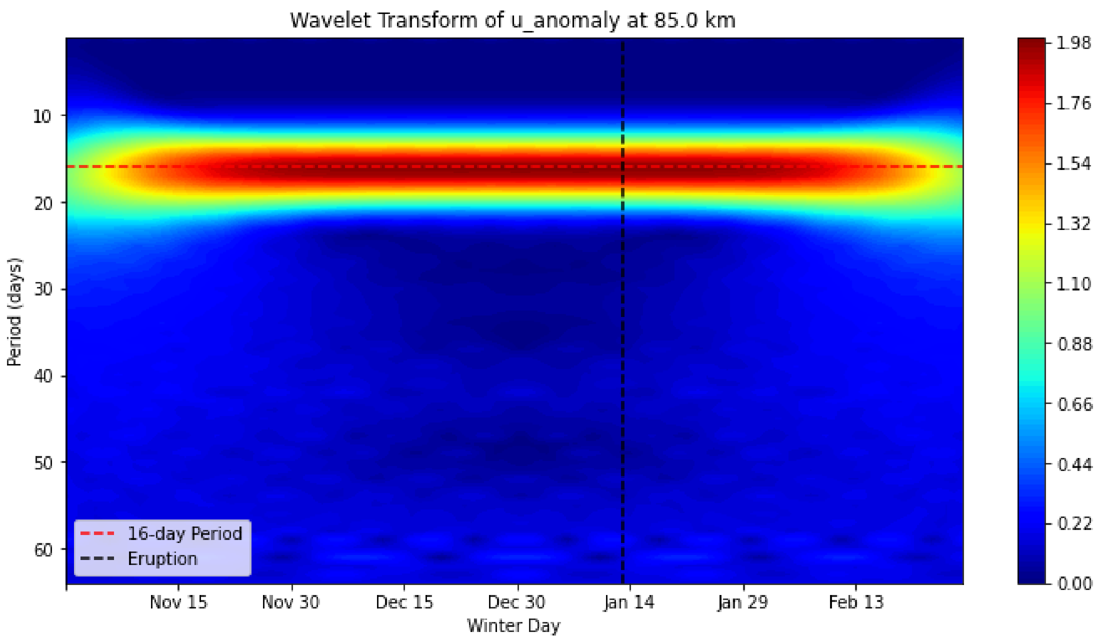

Figure 4.7.1: Wavelet of a sinus function with a 16-day period

Often it is beneficial to plot a few days together, so for example when looking at the 16-day wave, one plots the presence of the 12-18 day wave over time.

CHAPTER
FIVE

RESULTS AND DISCUSSION

5.1 Data Availability

The eruption period data contains some missing dates, the missing data were plotted and can be seen in Figure 5.1.1. The green indicates that there are available data for the date, while red indicates that there is no available data for that date.

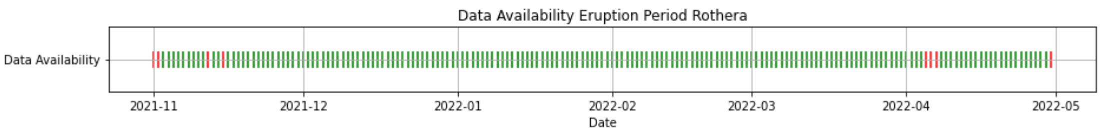

(a) Availability of data during the eruption period from Rothera. Red indicate no available data, while green indicates available data.

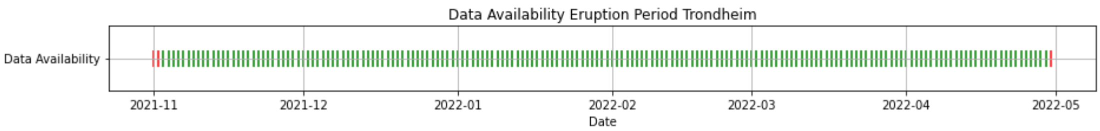

(b) Availability of data during the eruption period from Trondheim. Red indicate no available data, while green indicates available data.

Figure 5.1.1: Data availability for eruption periods

There are a total of eight days of missing data from the eruption period at Rothera:

- 2021-11-01
- 2021-11-02
- 2021-11-12
- 2022-11-15
- 2022-04-05
- 2022-04-06
- 2022-04-07
- 2022-04-30

The eruption period data at Trondheim have three dates with missing data:

- 2021-11-01
- 2021-11-02
- 2022-04-30

The climatologies in this thesis were calculated as a median over multiple years and only utilizes data that is available for a specific date. Therefore, the gaps in the data from Rothera and Trondheim are unlikely to significantly impact the overall climatology. However, it is worth highlighting that the climatologies, compiled using data from 2012 to 2023, does exhibit some missing points. Some of these points are also outside of the dates used in the climatology. As illustrated in Figure 5.1.2a, the missing data points from Rothera are primarily concentrated in 2018. The missing dates around 2022 is the eruption period, which is not included in the climatology. Figure 5.1.2b exhibits the dates with no data in the Trondheim data. There are some bulks of missing data, one in 2019 and one in 2021. However most of these will have no impact on the results, as the eruption period from 1 November until April 30 is the period of interest and much of the missing data is outsize this period.

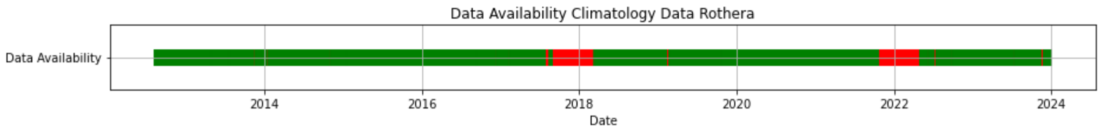

(a) Data availability of data used to make climatology Rothera

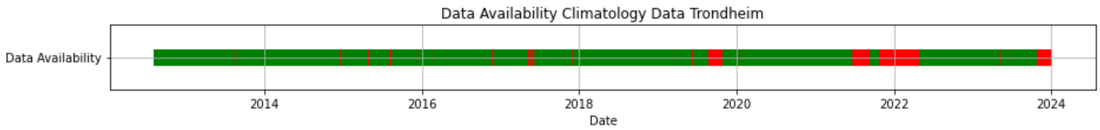

(b) Data availability of data used to make climatology Trondheim

Figure 5.1.2: Data availability used to make climatology

5.2 Results Mean Wind Rothera

The results for the mean wind measured at Rothera station are represented in this section.

5.2.1 Zonal Mean Wind Rothera

The climatology of the zonal mean wind measured from the Rothera radar is shown in Figure 5.2.1a. During the summer months, November to February, there is a peak in negative wind values at lower altitudes, indicating a westward flow. At the same time, there is an eastward flow at higher altitudes creating a wind shear. This observation is consistent with other studies conducted in the southern hemisphere, such as Hibbins et al. (2005)[22], who observed similar seasonal wind patterns in the mesosphere.

The anomaly plot (daily data-climatology) in Figure 5.2.1b shows deviations from the climatology during the eruption period. The white areas are periods with no available data for the eruption period, they correspond with the dates found in Figure 5.1.1a in Section 5.1. This is the case for all the following anomaly plots using data from Rothera. The anomaly plot suggests the presence of a 16-day wave at higher altitudes post-eruption.

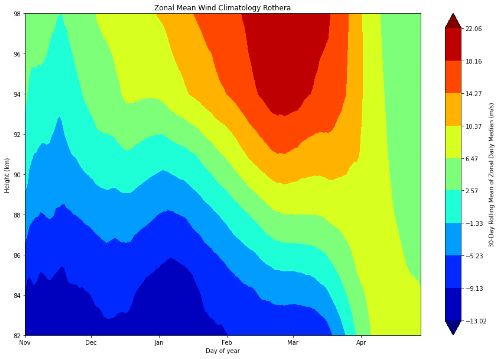

(a) Climatology of the zonal mean wind with 30-day rolling mean.

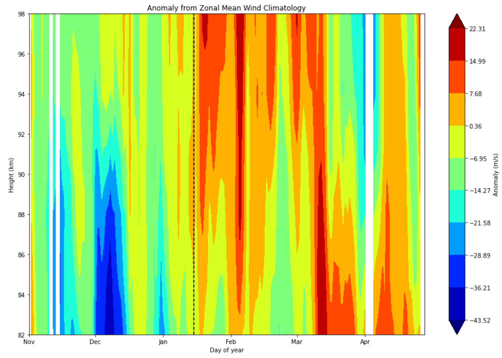

(b) Anomaly of the eruption period zonal mean wind compared to the climatology. Vertical dashed line indicates date of eruption January 15.

Figure 5.2.1: Zonal mean wind analysis Rothera

5.2.2 Lomb-Scargle Periodogram Zonal Mean Wind Anomaly Rothera

The Lomb-Scargle periodogram of the zonal mean wind anomaly (Figure 5.2.2) reveals peaks around the 16-day frequency at the altitudes 94km and 98km. This suggests the presence of a 16-day wave, consistent with the anomaly plot in Figure 5.2.1b. However, it does also include several other peaks, for the Lomb-Scargle at 98km there is higher peaks indicating an 11-day wave and a 8-day wave, these are also present at 94km altitude.

5.2.3 Wavelet Zonal Mean Wind Anomaly Rothera

To further investigate the possibility that there is a 16-day wave present, a wavelet analysis was carried out. The results are shown in Figure 5.2.3. For the altitudes 94km and 98km, there are some presence of a 16-day wave that appear aroundt the time of the eruption, which is marked by the dashed vertical line.

To get a closer look, the extracted 16-day wave was plotted for the altitudes 94km and 98km. The extracted wave is the mean of the 12-18 day wave intensity, as the 16-day planetary wave not necessarily is exactly 16-days. This can be seen in Figure 5.2.4. Here, it is evident that the increase in the presence of the 16-day wave started before the eruption. Therefore, it is not possible to attribute the 16-day wave to the eruption with certainty for the zonal mean wind anomaly.

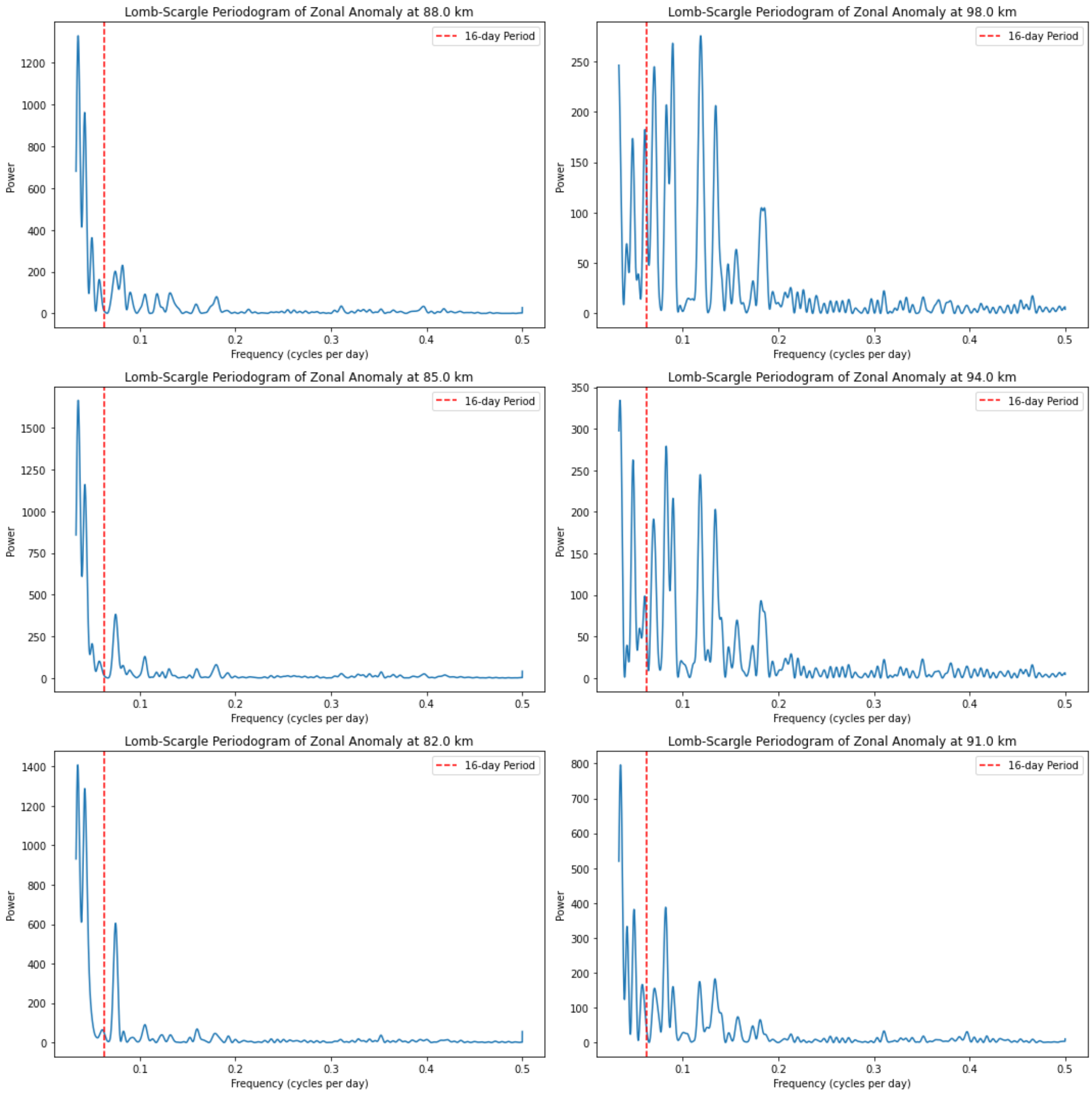

Figure 5.2.2: Lomb-Scargle periodogram of the zonal mean wind anomaly Rothera for heights between 82 and 98km.

5.2.4 Meridional Mean Wind Rothera

The climatology of the meridional mean wind is depicted in Figure 5.2.5a. The positive values during December to February indicate a northward wind, which shifts to a southward flow by April. This is consistent with other studies conducted in the southern hemisphere[22]. This pattern aligns with typical seasonal atmospheric circulation changes.

The anomaly plot (daily data-climatology) in Figure 5.2.5b show how the eruption period differs from the climatology. Similar as for the zonal anomaly results in Figure 5.2.1b, there is also a reason to suspect a 16-day wave for the meridional mean wind anomaly. However, here it looks to be present from before the eruption. It could be interesting to investigate if the wave is affected by the eruption, and therefore it was done a Lomb-Scargle periodogram.

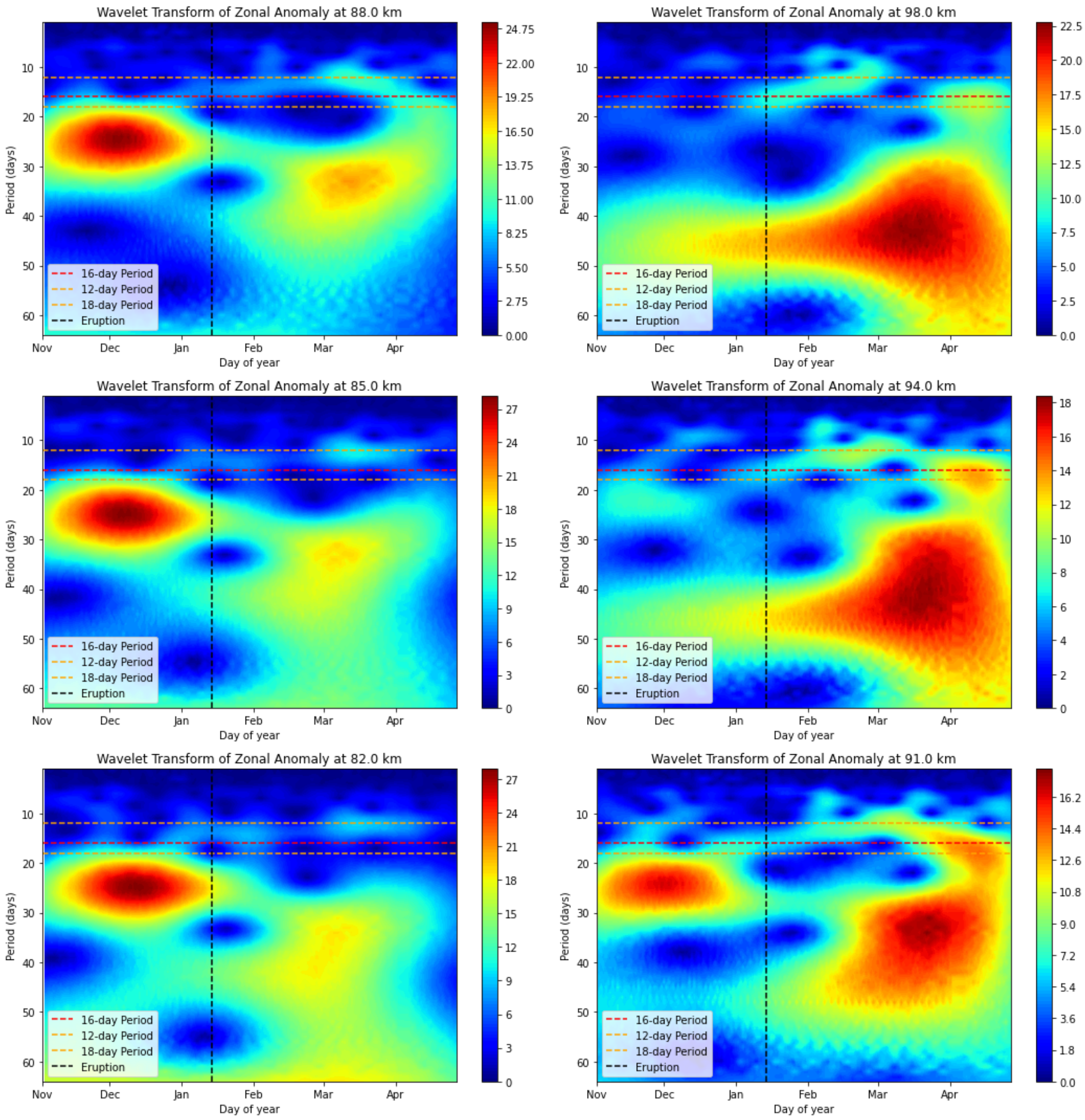

Figure 5.2.3: Wavelet of the zonal mean wind anomaly for heights 82km,85km, 88km, 91km, 94km and 98km

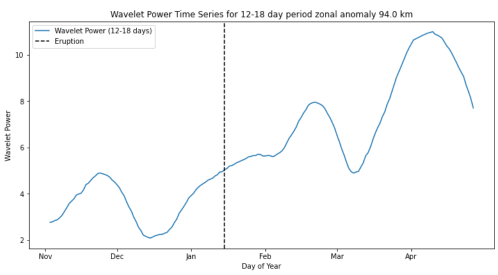

(a) 94km altitude

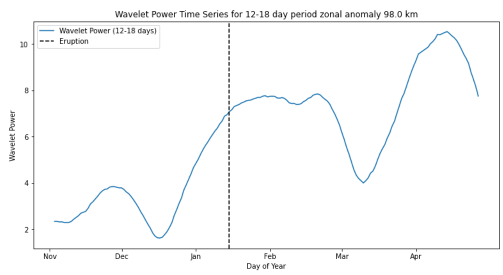

(b) 98km altitude

Figure 5.2.4: 16-day wave analysis, using extracted wavelet values from 12-18 day period, at a) 94km and b) 98km altitudes for the zonal mean wind anomaly.

5.2.5 Lomb-Scargle Periodogram Meridional Mean Wind Anomaly Rothera

The Lomb-Scargle periodogram (Figure 5.2.6) shows a clear 16-day wave at 82 km, while the other altitudes seems to have clear peaks for both higher and lower

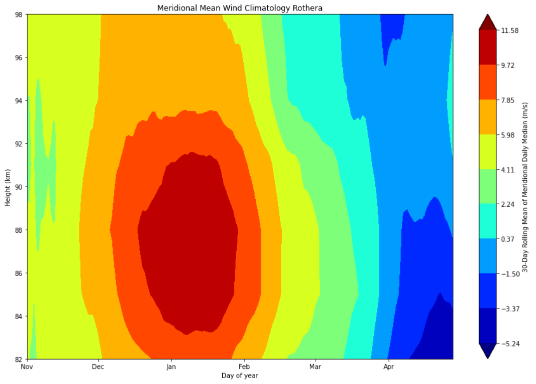

(a) Climatology of the meridional mean wind with 30-day rolling mean.

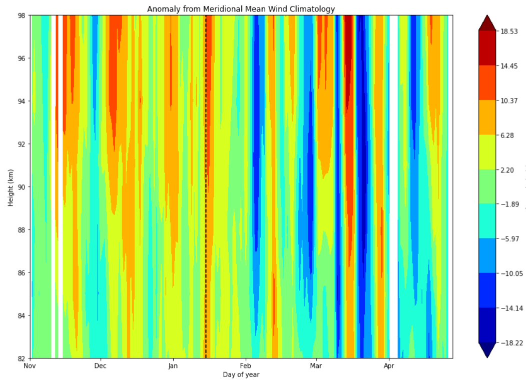

(b) Anomaly of the eruption period meridional mean wind compared to the climatology. Vertical dashed line indicates date of eruption January 15.

Figure 5.2.5: Meridional mean wind analyzis.

frequencies.

5.2.6 Wavelet Meridional Mean Wind Anomaly Rothera

To examine the evolution of the 16-day wave found in Figure 5.2.6 over time, a wavelet analysis was conducted. The wavelet analysis (Figure 5.2.7) shows a pronounced 16-day wave and fewer disturbances compared to the zonal wind analysis.

The extracted 16-day wave at 82 km altitude in Figure 5.2.8 indicates an increase in the presence of a 16-day wave after the eruption. This observation can be attributed to the dynamical processes in the stratosphere and their coupling to the mesosphere and lower thermosphere (MLT), as the increase does not happen immediately after the eruption.

In March 2022, both a Stratospheric Final Warming (SFW) and a Sudden Stratospheric Warming (SSW) occurred in the Northern Hemisphere (NH). These events can significantly impact the 16-day wave[23]. The SSW, characterized by a rapid reversal of the polar vortex winds and a substantial warming of the stratosphere, can inject planetary wave momentum into the stratosphere. When these waves break, they deposit westward momentum, slowing down or even reversing the typically eastward winter polar vortex winds. This process can temporarily create a "summer-like" condition in the winter polar stratosphere, allowing mid-latitude warm air to penetrate the polar region.

The interhemispheric coupling plays a crucial role here. The dynamical disturbances caused by the SSW in the NH can propagate across the equator and influence the Southern Hemisphere (SH) stratosphere and MLT regions [24, 25]. This coupling can explain the observed 16-day wave enhancements in the SH, even though the primary stratospheric warming events occurred in the NH.

Moreover, as the final warming approaches, the polar vortex winds naturally weaken. Even relatively weak planetary waves, which might not reverse the strong mid-winter vortex winds, can significantly impact the weaker winds near the final warming. This scenario can lead to a sudden stratospheric warming near the final warming, making it challenging to distinguish between an early final warming and

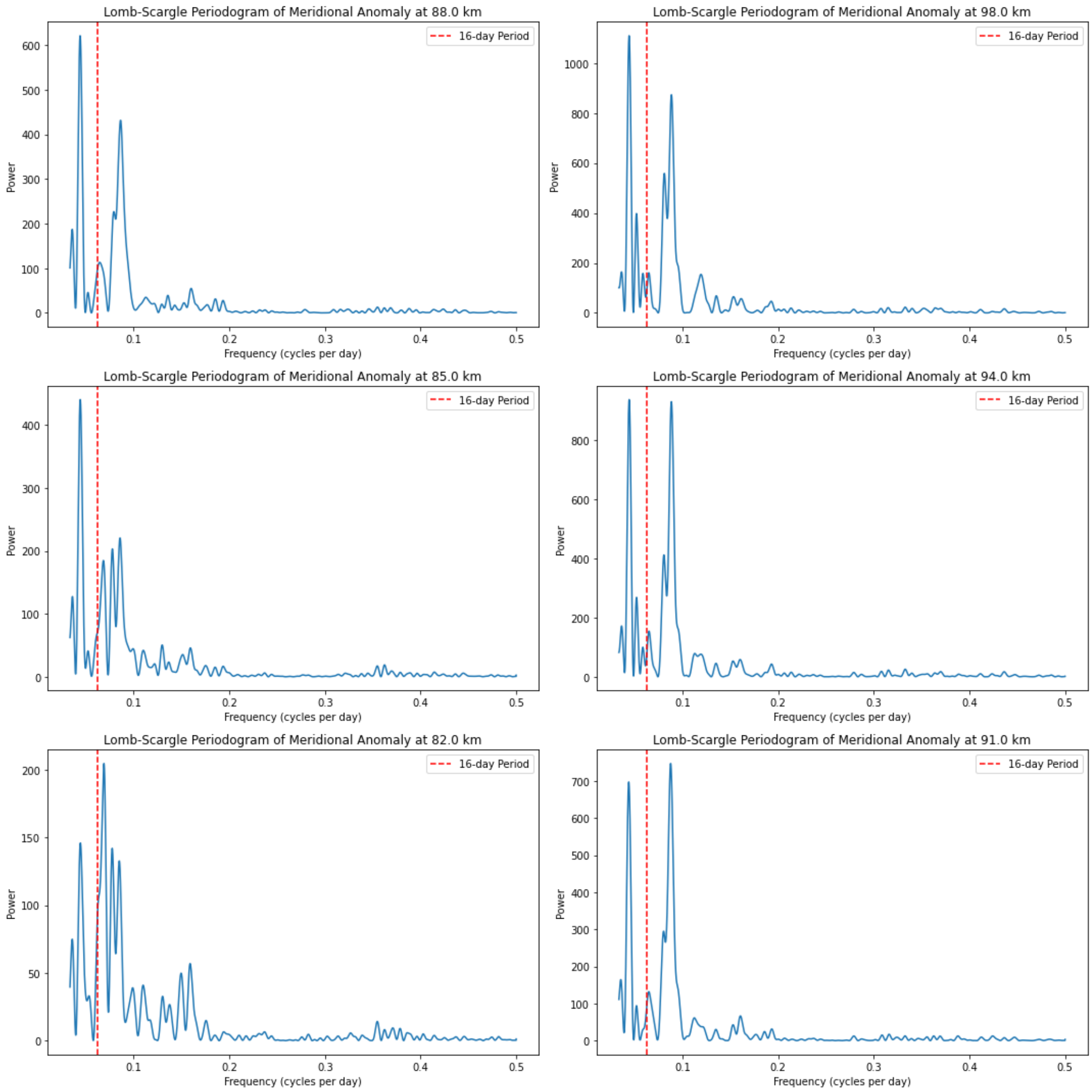

Figure 5.2.6: Lomb-Scargle periodogram of the meridional mean wind anomaly Rothera for heights between 82 and 98km.

an SSW followed by the seasonal final warming.

The increase in 16-day wave activity at 82 km altitude post-eruption may thus be linked to these complex dynamical interactions. The presence of both SFW and SSW events in the NH around March 2022 likely contributed to this enhanced planetary wave activity observed in the SH. These findings align with previous studies indicating that SSW events can enhance planetary wave activity in the MLT[26, 27].

5.3 Results 12h Amplitude Rothera

The results for the 12h amplitude with data from Rothera are presented here.

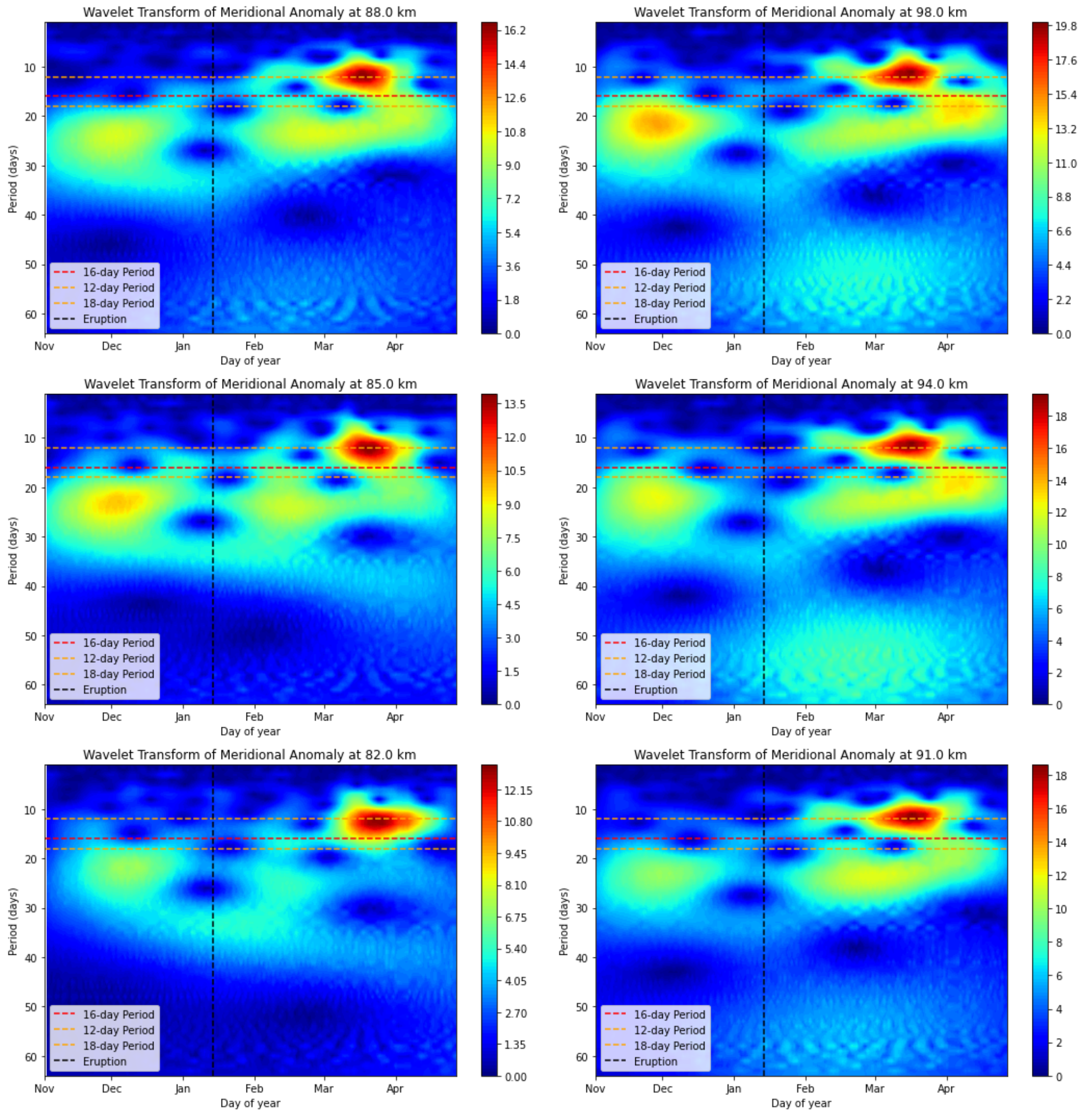

Figure 5.2.7: Wavelet of the meridional mean wind anomaly for heights 82km,85km, 88km, 91km, 94km and 98km

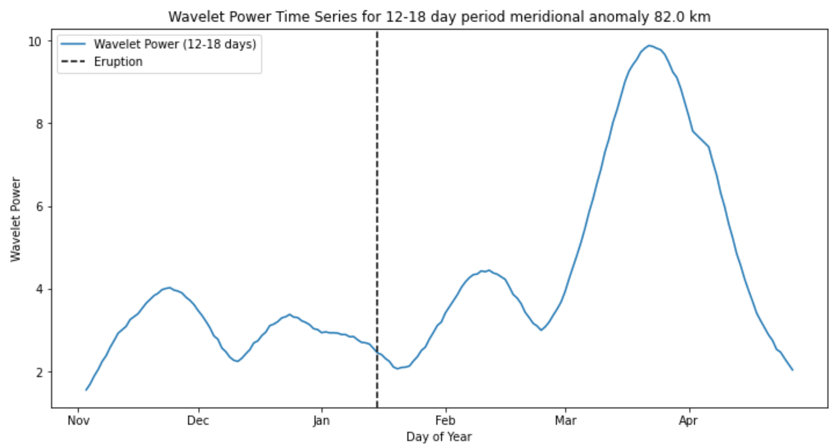

Figure 5.2.8: 16-day wave analysis, using extracted wavelet values from 12-18 day period, at 82km altitude for the meridional mean wind anomaly. The vertical black dashed line marks day of the eruption.

5.3.1 Zonal 12h Amplitude Rothera

The zonal 12h amplitude is illustrated in Figure 5.3.1a, while the anomaly from the 12h amplitude from the eruption period is in Figure 5.3.1b. The trends of the zonal 12h amplitude climatology are in line with the results of Hibbins et al. (2007) [28].

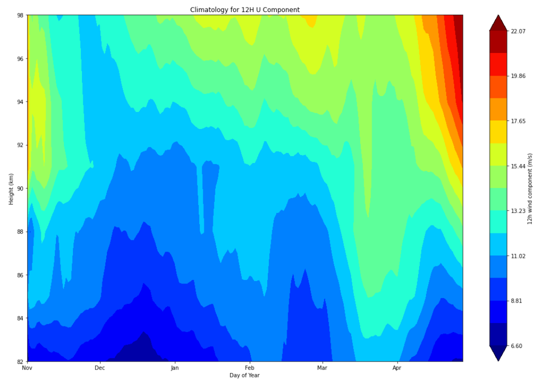

(a) Climatology of the zonal 12h amplitude.

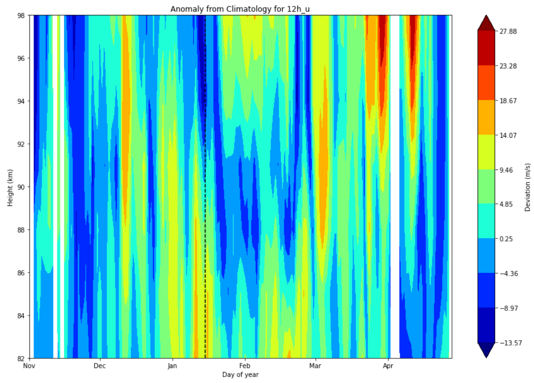

(b) Anomaly of the eruption period zonal 12h amplitude compared to the climatology. The vertical black dashed line marks day of the eruption.

Figure 5.3.1: Zonal 12h amplitude climatology and anomalies for the eruption period with data from Rothera

In the anomaly plot (Figure 5.3.1b), it is harder to see whether there is a 16-day wave present or not. Therefore, a Lomb-Scargle Periodogram is necessary to investigate further.

5.3.2 Lomb-Scargle Periodogram Zonal 12h Amplitude Rothera

In the Lomb Scargle periodograms of the 12h amplitude in zonal direction in Figure 5.3.2, there seems to be a pretty clear 16-day wave for 85km altitude. There is also tendencies that indicate the presence of a 16-day wave for the other altitudes as well.

5.3.3 Wavelet Zonal 12h Amplitude Anomaly Rothera

The Lomb-Scargle periodogram suggested potential interesting results in the wavelet analysis. However, the wavelet analysis (Figure 5.3.3) is full of bursts, which complicates the extraction of meaningful insights. This issue may arise from the high variability in the anomaly data, which challenges the wavelet's ability to properly decompose the signal.

Rapid increases and decreases in the data, occurring over a few days, can result in a "streak" of low to high frequencies in the wavelet transform. This phenomenon is particularly pronounced in the presence of pulses, which are characterized by sudden changes in the data. Consequently, the strong variability in the 12-hour zonal amplitude suggests that other analytical techniques might be necessary.

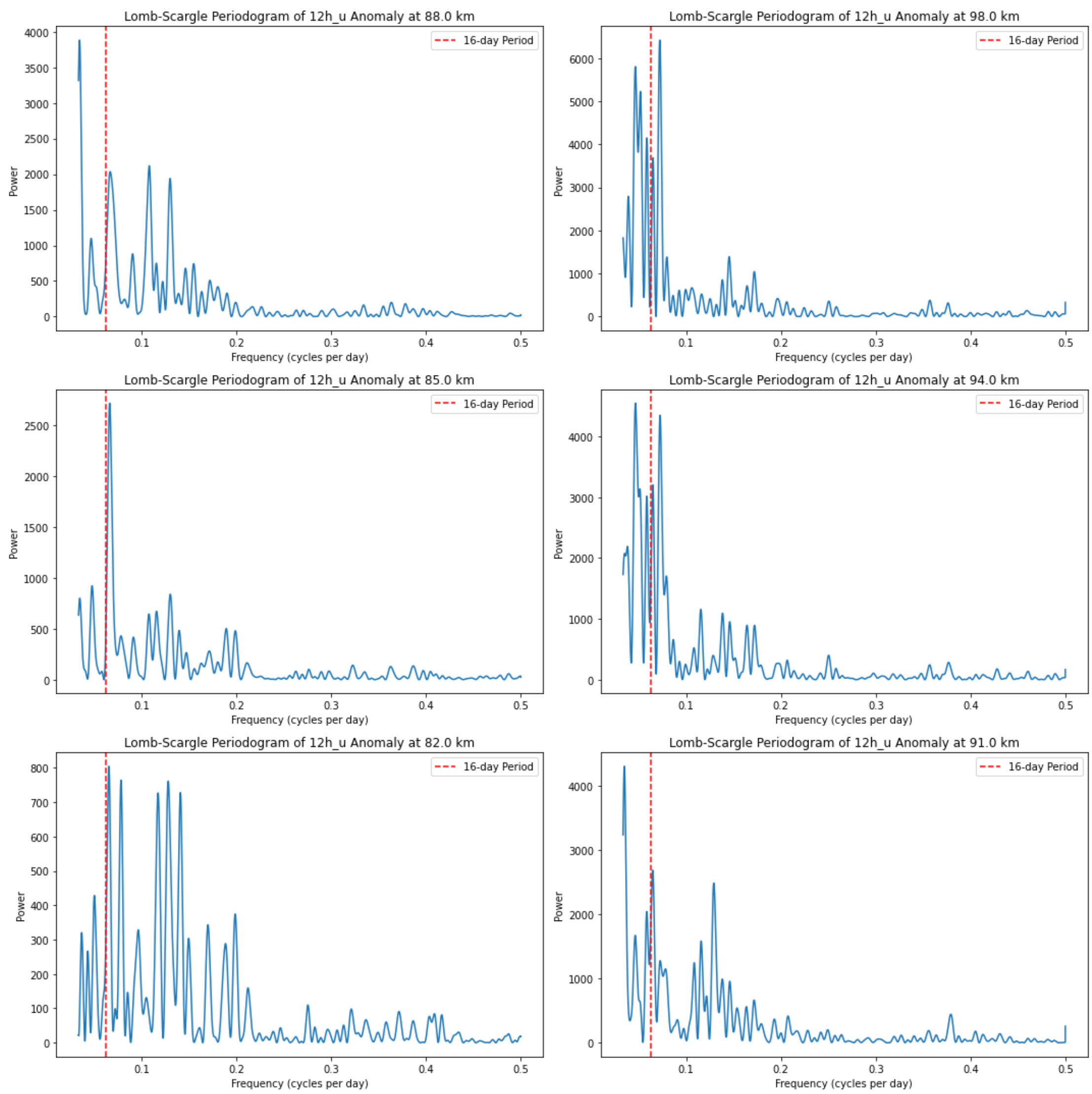

Figure 5.3.2: Lomb-Scargle periodogram for the zonal 12h amplitude for the altitudes 82, 85, 88, 91, 94 and 98km. Red dashed line is 16-day frequency.

Various wavelets, such as 'Paul' and 'Mexican hat', were tested, but all showed similar bursts.

Significant power in the wavelet transform does not necessarily indicate the presence of a periodic signal. Every waveform has a Fourier equivalent, which displays power at various frequencies. This does not imply actual periodicity at those frequencies in the data.

The variability observed in the wavelet analysis highlights the need for alternative analytical approaches. Techniques such as the Stockwell Transform, which offers better window control, could potentially provide clearer insights into the true characteristics of the data[29].

5.3.4 Meridional 12h Amplitude Rothera

The meridional 12h amplitude climatology is showed in 5.3.4a, just like the zonal 12h amplitude climatology, the meridional 12h climatology also have trends similar

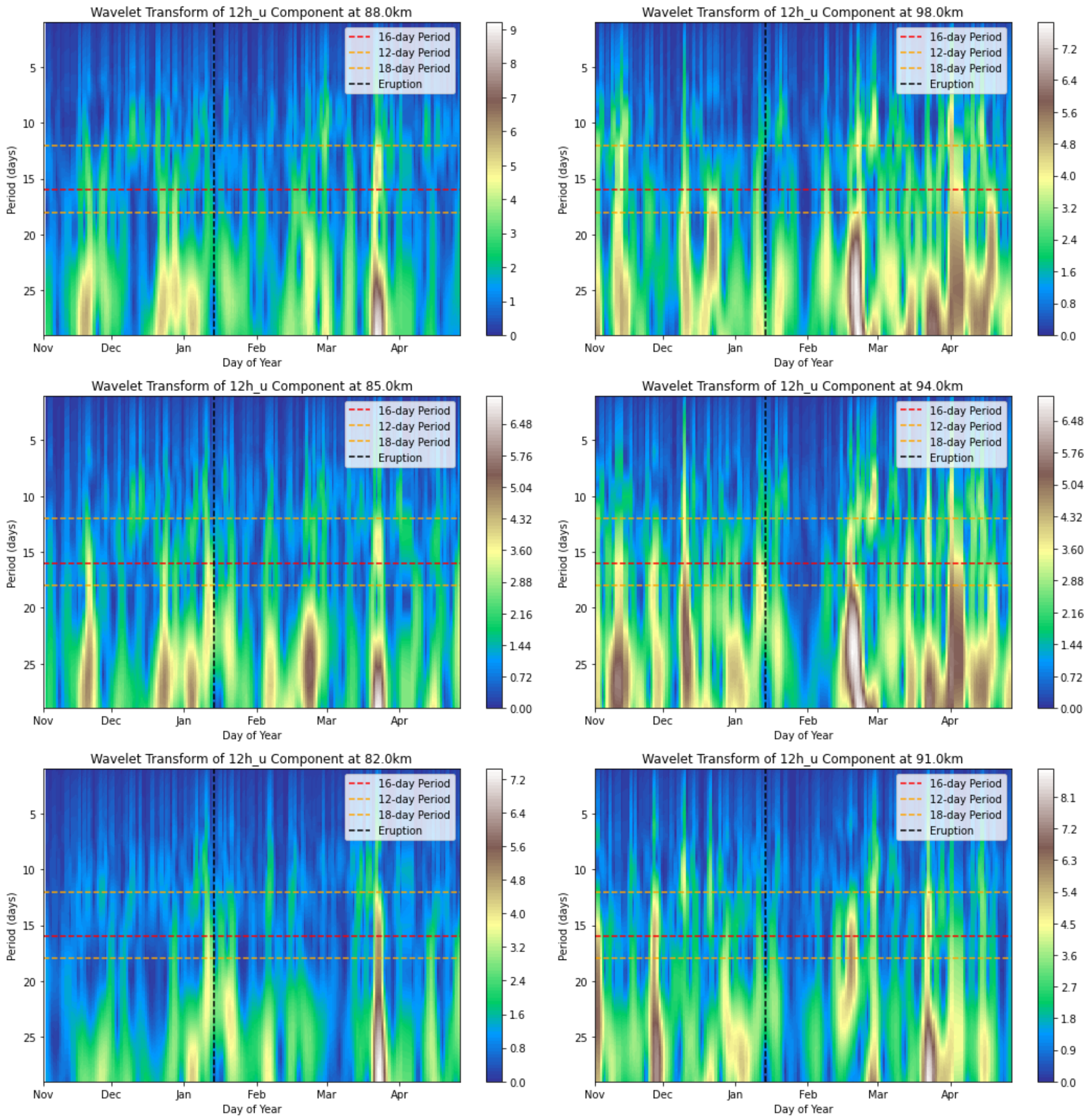

Figure 5.3.3: Wavelet of the zonal 12h amplitude, the red dashed line is the 16-day period, the two orange marks the 12- adn 18-day period, while the black dashed line is the eruption date.

as the ones in the study by Hibbins et al. (2007) [28]. For the anomaly plot (Figure 5.3.4b), it looks like a 16-day wave appears after the eruption for the higher altitudes.

5.3.5 Lomb-Scargle Periodogram Meridional 12h Amplitude Rothera

The Lomb-Scargle periodogram (Figure 5.3.5) confirms the presence of a 16-day wave at 82 km and 85 km, and some close to 16-day period wave for 94km and 98km. However, further analysis is needed to understand its development over time.

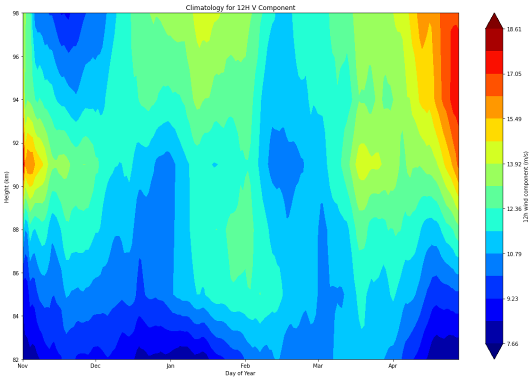

(a) Climatology of the meridional 12h amplitude Rothera

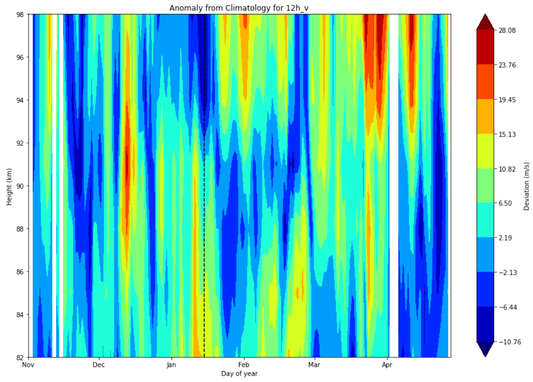

(b) Anomaly of the eruption period meridional 12h amplitude compared to the climatology. The vertical black dashed line marks day of the eruption.

Figure 5.3.4: Meridonal 12h amplitude analysis at Rothera.

5.3.6 Wavelet Meridional 12h Amplitude Rothera

The wavelet analysis (Figure 5.3.6) for the meridional 12h amplitude exhibits multiple bursts, similar to the zonal 12h amplitude wavelet (Figure 5.3.3). There are potential wave patterns near the 10-day horizontal line. However, to gain a clearer understanding of these waves, it would be necessary to employ different analytical methods for verification, as discussed in Section 5.3.3.

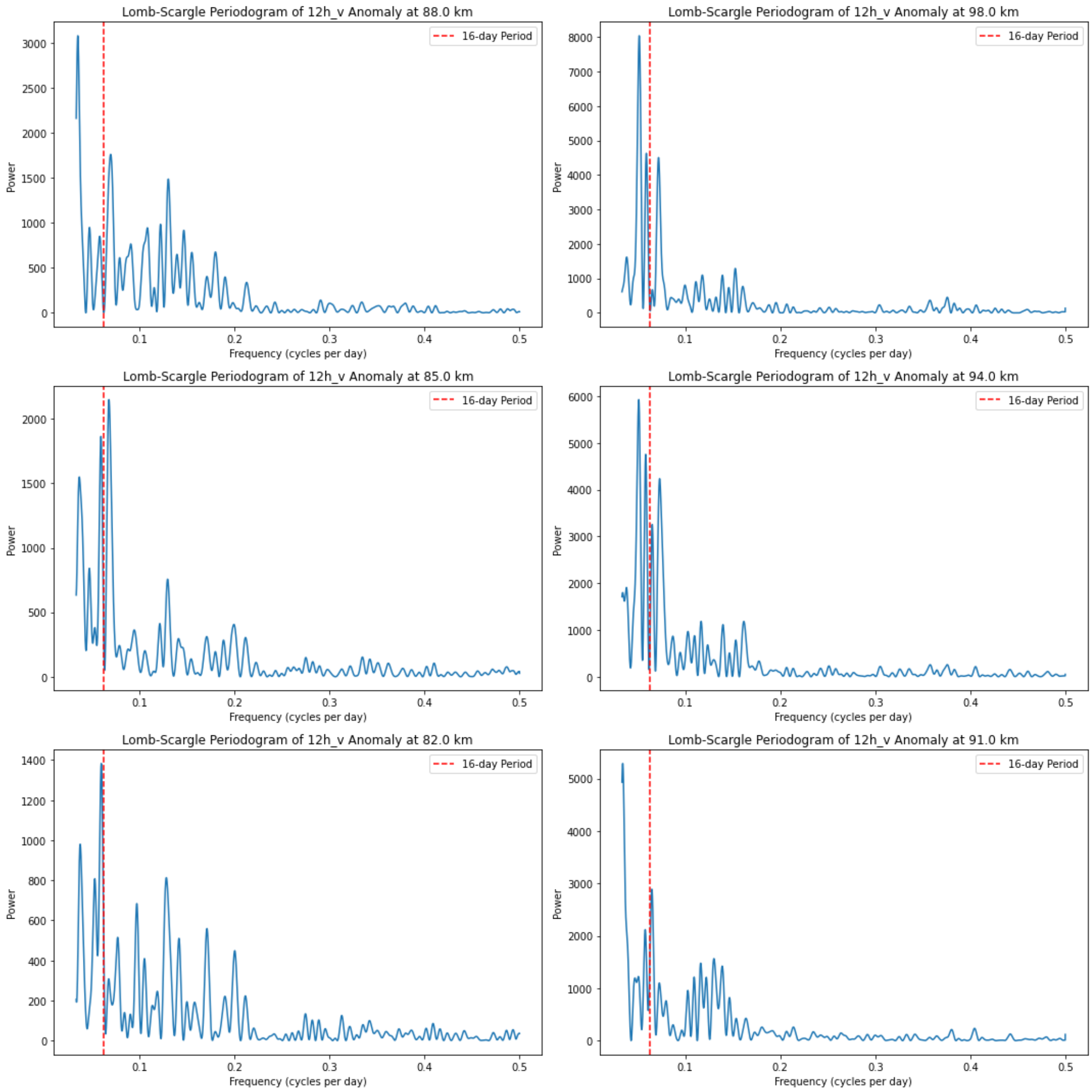

Figure 5.3.5: Lomb-Scargle periodogram for the meridional 12h amplitude for the altitudes 82, 85, 88, 91, 94 and 98km. Red dashed line is 16-day frequency.

5.4 Results Mean Wind Trondheim

The results for the mean wind measured at Dragvoll in Trondheim are represented in this section.

5.4.1 Zonal Mean Wind Trondheim

The zonal mean wind (Figure 5.4.1a) have eastward winds for the winter periods, and the winds change direction going towards summer. This is comparable to the findings of Sandford et al. (2010), where the mean winds over Esrange is plotted in a climatology similar to the one in Figure 5.4.1a [30]. The winds over Esrange have the same shift to negative values, happening around the end of March/beginning of April. Elsewhere the values are positive.

The anomaly plot 5.2.1b have some wave patterns, and have a strong deviation at the time of eruption.

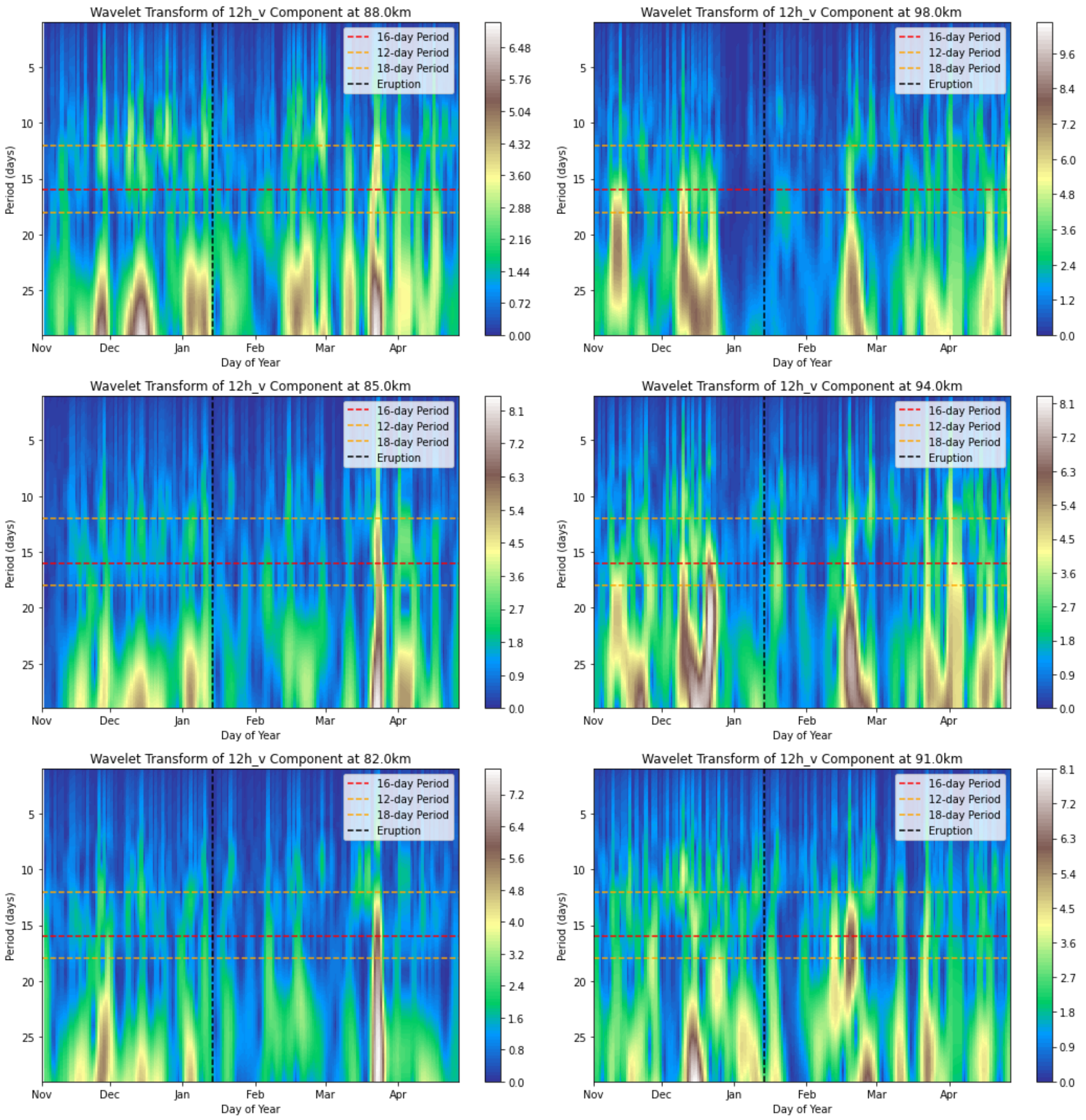

Figure 5.3.6: Wavelet of the meridional 12h amplitude, the red dashed line is the 16-day period, the orange lines are the 12- and 18-day period, while the black vertical dashed line is the eruption date.

5.4.2 Lomb-Scargle Periodogram Zonal Mean Wind Trondheim

The Lomb-Scargle periodogram (Figure 5.4.2) shows a clear 16-day wave at all altitudes, with some shorter frequency waves also present.

5.4.3 Wavelet Zonal Mean Wind Anomaly Trondheim

The evolution of the 16-day wave for the zonal mean wind in Trondheim can be seen in Figure 5.4.3. The 16-day wave seems to be present before the eruption for all the different altitudes. Therefore, there is not possible to tell if the eruption is doing something with the wave.

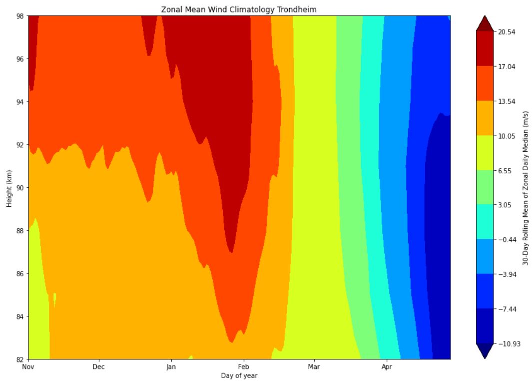

(a) Climatology of the zonal mean wind with 30-day rolling mean.

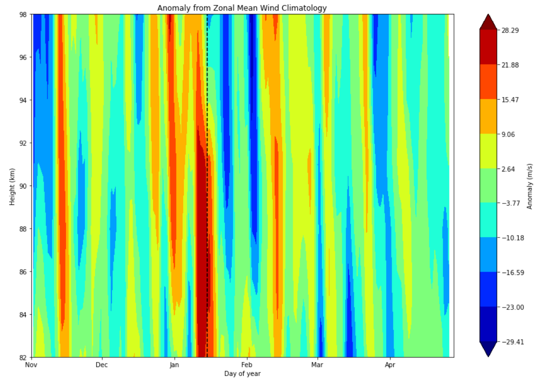

(b) Anomaly of the eruption period zonal mean wind compared to the climatology. Vertical dashed line indicates date of eruption January 15.

Figure 5.4.1: Analysis of zonal mean wind and the anomalies for the eruption period at Dragvoll in Trondheim

5.4.4 Meridional Mean Wind Trondheim

The meridional climatology in Figure 5.4.4a, indicates that the mean winds are mostly pointing towards north for the winter and the winds are turning southward going towards the summer. Summertime winds in both hemispheres will point equatorward, this is the case here. It is noteworthy that the meridional winds mostly turns positive during November and February, this is the case for the results in Figure 5.4.4a, and is also the case for the results by Sandford et al. (2010)[30]. The temperatures of the MLT form Rothera and Trondheim can be seen in Figure 5.4.5. One can tell that the temperatures of the two hemispheres have similar trends for the seasons. However, the results for the Northern hemisphere (NH) is much less steady than the temperatures in the Southern hemisphere (SH). This could be the effect of large deviations due to sudden stratospheric warming events (SSW) that are common in the NH but rare in the SH. The meridional winds and temperature are related, which can explain the variations in the climatology. The variations of the climatology can also be seen in the Appendix 6, where the raw data have been plotted and one can see the difference between the climatologies from the NH and SH.

The anomaly for the climatology in Figure 5.4.4b, shows signs of a 16-day wave presence, specially after the eruption.

5.4.5 Lomb-Scargle Periodogram for the Meridional Mean Wind Anomaly

The Lomb-Scargle periodogram (Figure 5.4.6) confirms the presence of a 16-day wave across all altitudes, and a wavelet is necessary to understand the evolution of this wave.

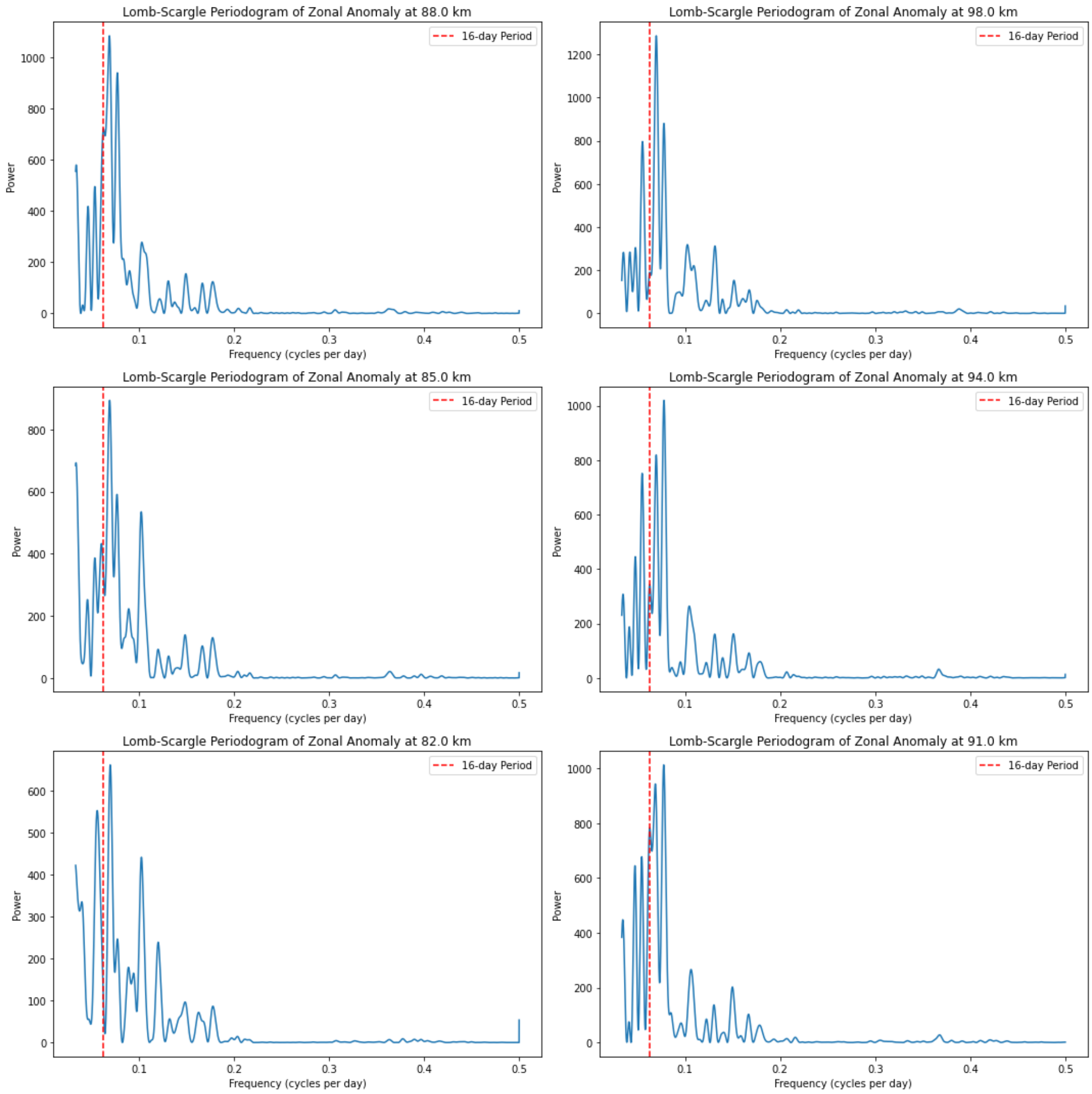

Figure 5.4.2: Lomb-Scargle peridogram of the zonal mean wind in Trondheim. Dashed red line indicate 16-day period wave

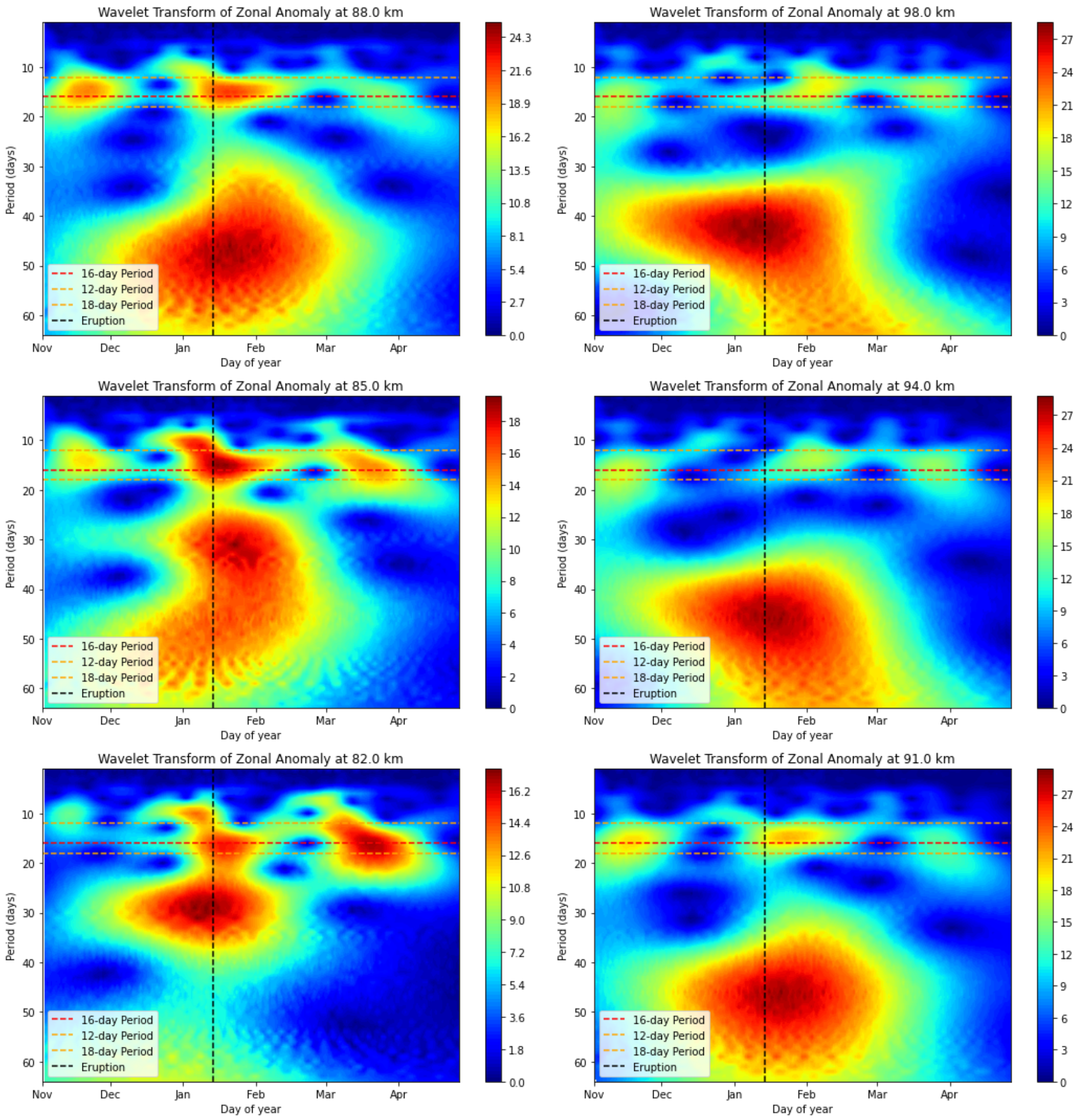

Figure 5.4.3: Wavelet of the zonal mean wind anomaly in Trondheim. The red dashed line is the 16-day period, the orange lines are the 12- and 18-day period, while the black vertical dashed line is the eruption date.

5.4.6 Wavelet Meridional Mean Wind Anomaly Trondheim

The wavelet analysis (Figure 5.4.7) shows the 16-day wave around the eruption period, suggesting a possible correlation between the eruption and the planetary wave. However, there is also a possibility that the 16-day wave increase happens before the eruption.

To further look into the possibility of the 16-day wave being related to the eruption, Figure 5.4.8 shows the extracted 16-day wave is for selected altitudes 85km, 88km, 94km and 98km. Here there is hard to conclude if the eruption affects the 16-day wave, as there for 85 and 88km seems to start an increase before, and for 94 and 98km it is hard to know whether the increase would have happened ether way or if the eruption is at fault.

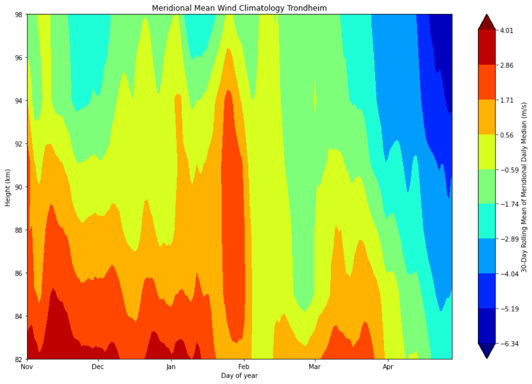

(a) Climatology of the meridional mean wind measured at Dragvoll in Trondheim

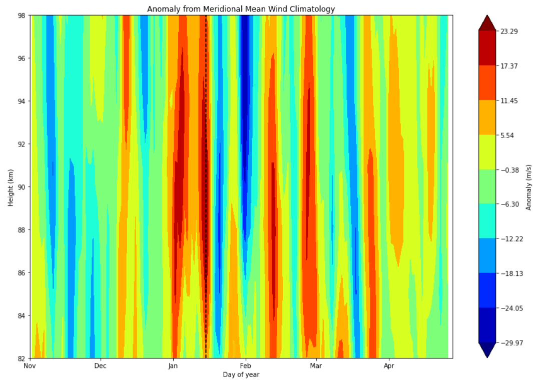

(b) Meridional anomaly of the eruption period compared to the climatology Trondheim. The vertical black line indicates the day of the eruption.

Figure 5.4.4: Meridional mean wind and anomalies for the eruption period at Dragvoll in Trondheim

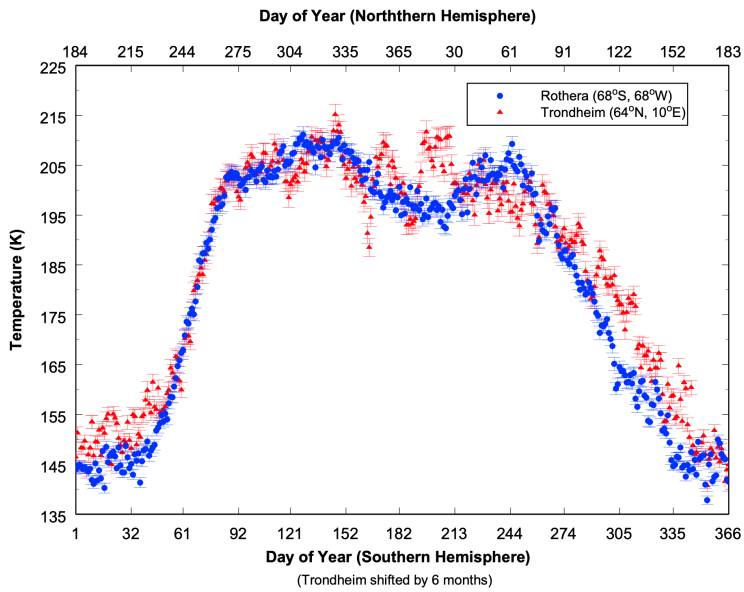

Figure 5.4.5: Yearly temperatures for Rothera and Trondheim (Trondheim shifted by 6 months to line up seasons in the NH and SH). Figure is used with permission from Patrick J. Espy.

5.5 Results 12h Amplitude Trondheim

The results for the 12h amplitude with data from Dragvoll in Trondheim are represented in this section.

5.5.1 Zonal 12h Amplitude Trondheim

The climatology for the zonal 12-hour amplitude is shown in Figure 5.3.1a. Portnyagin et al. (1993) study the semidiurnal tide at Poker flat, which have similar

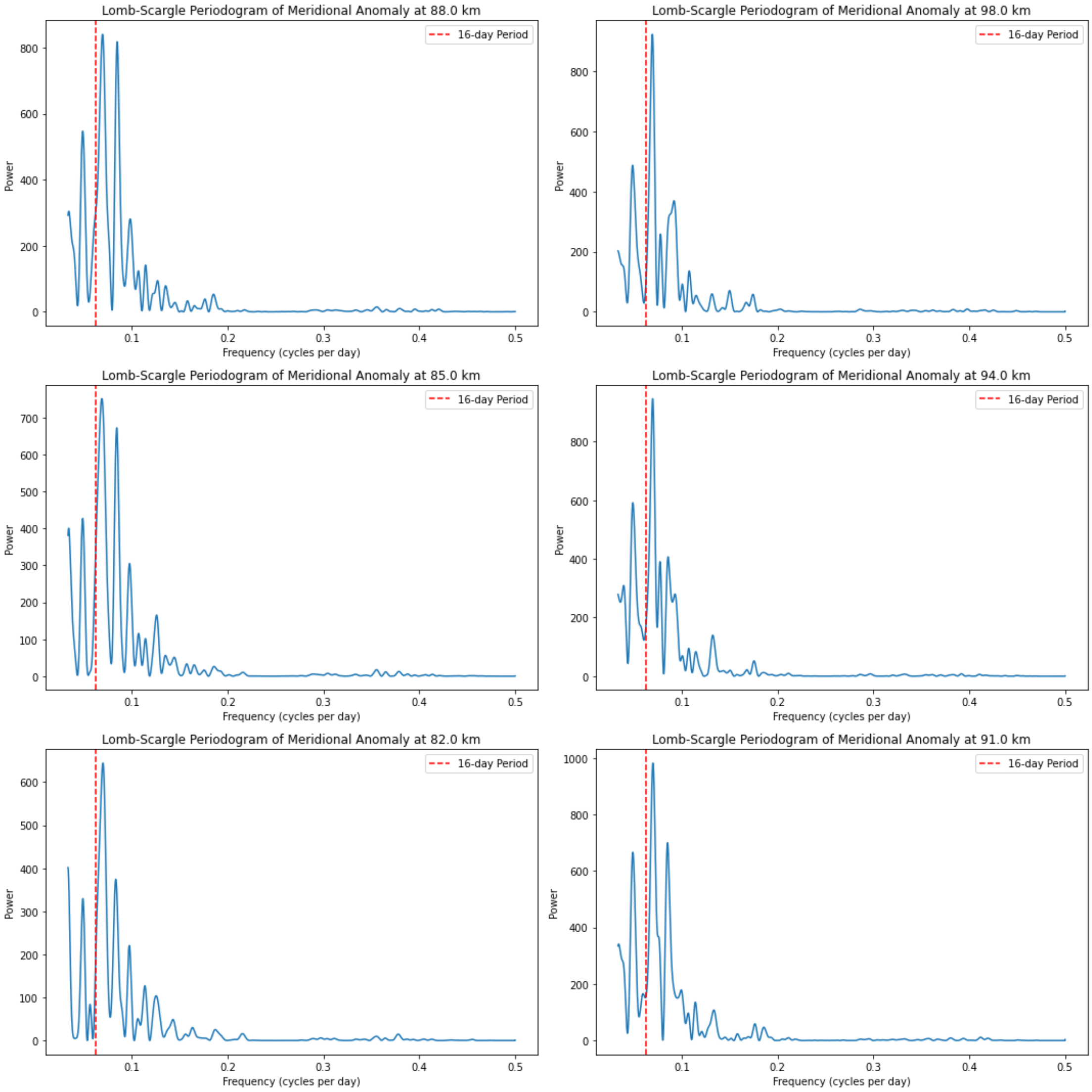

Figure 5.4.6: Lomb-Scargle peridogram of the meridional mean wind in Trondheim.

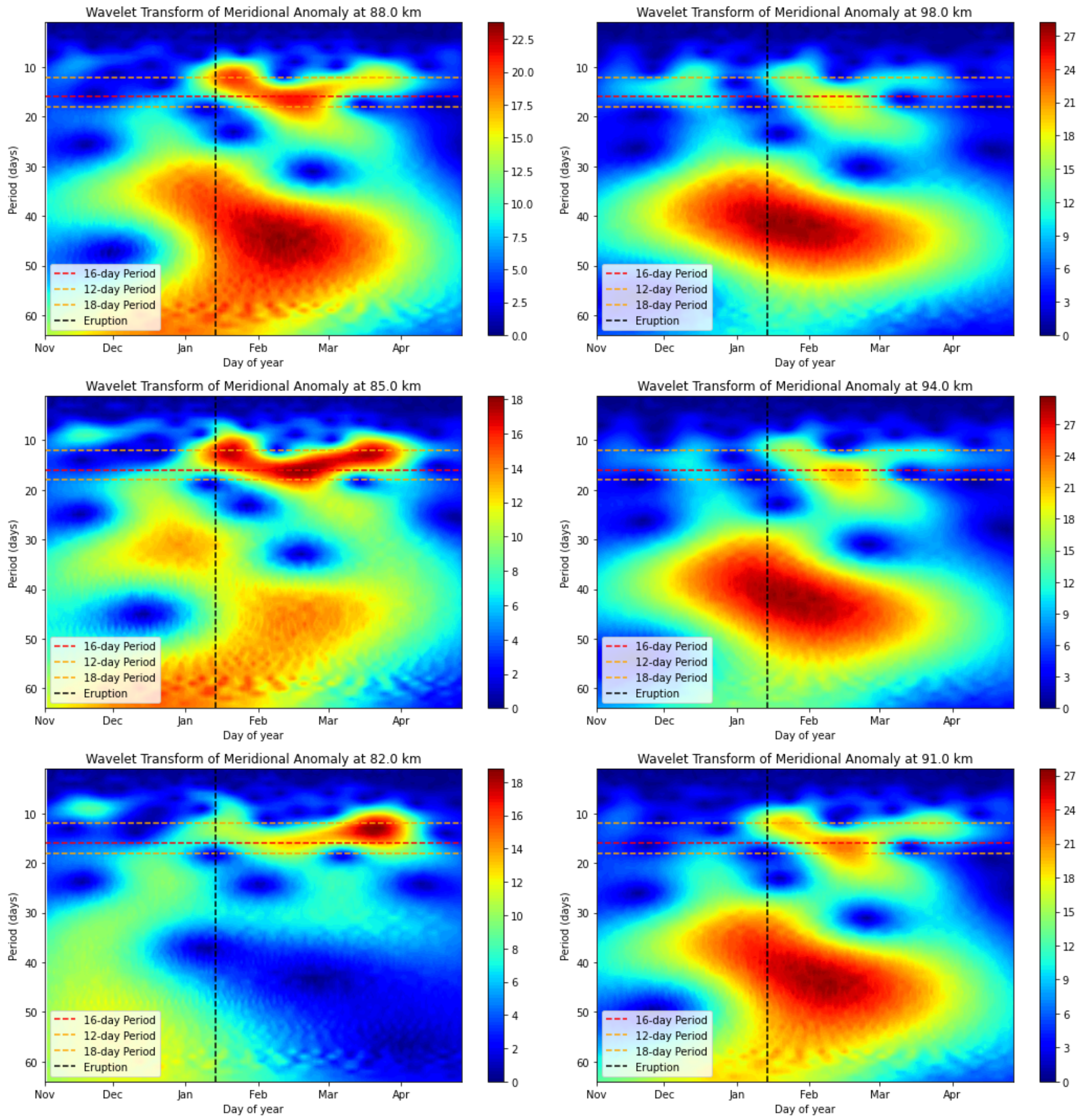

Figure 5.4.7: Wavelet of the meridional mean wind anomaly in Trondheim. The red dashed line is the 16-day period, the orange lines are the 12- and 18-day period, while the black vertical dashed line is the eruption date.

latitude as Trondheim[31]. Both studies show higher amplitudes at higher altitudes in the zonal direction. In Portnyagin et al. (1993), there are used a much heavier smoothing, and the study is looking at collective data from multiple radars. That can explain the differences in shape of the climatologies. The differences in amplitude values also have an reasonable explanation, as the amplitudes will differ a lot from location to location and if you are looking at migrating or non migrating waves etc. That can explain why the climatology from poker flat measured weaker amplitudes than this study did from the radar at Dragvoll[31].

Figure 5.5.1b showcase the anomaly of the climatology and the eruption period. It is some wave pattern fomming. However, it appears to be waves of longer periods than 16-days.

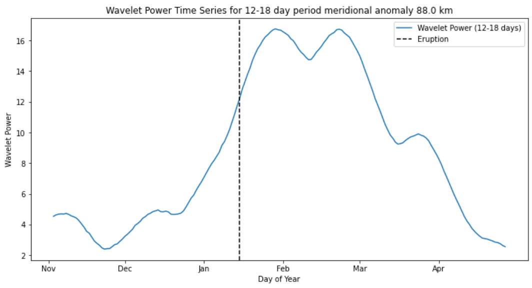

(a) Extracted 16-day wave for the meridional mean wind anomaly wavelet at 88km altitude.

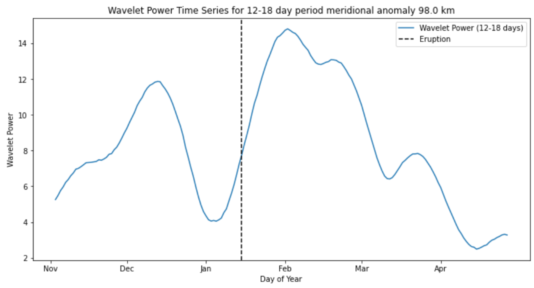

(b) Extracted 16-day wave for the meridional mean wind anomaly wavelet at 98km altitude.

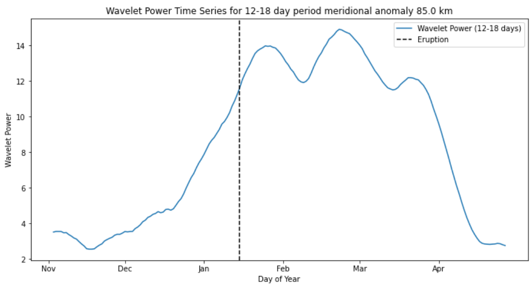

(c) Extracted 16-day wave for the meridional mean wind anomaly wavelet at 85km altitude.

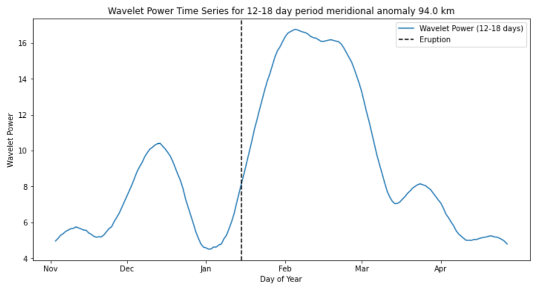

(d) Extracted 16-day wave for the meridional mean wind anomaly wavelet at 94km altitude.

Figure 5.4.8: Extracted 16-day wave for the meridional mean wind anomaly wavelet at various altitudes. The vertical black line indicates the date of the eruption.

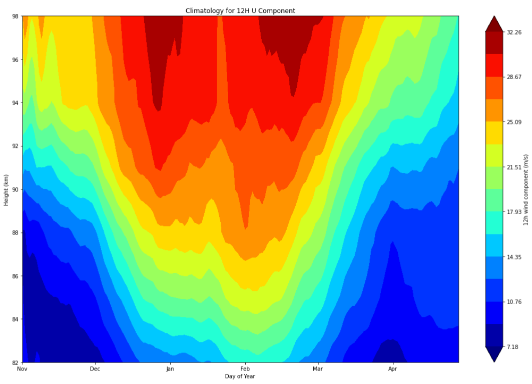

(a) Zonal climatology of the 12h amplitude in Trondheim

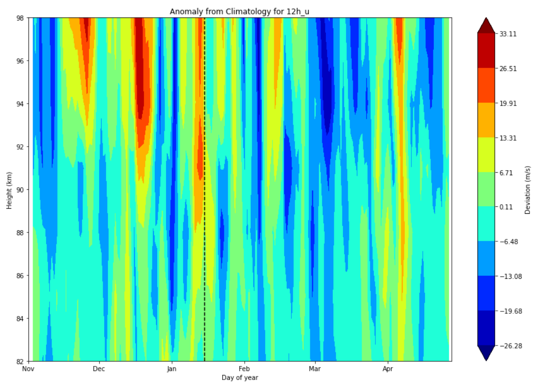

(b) Anomaly of the eruption period zonal 12h amplitude compared to the climatology

Figure 5.5.1: Zonal anomaly of the 12h amplitude in the eruption period compared to the climatology. The vertical black line indicates the time of the eruption.

5.5.2 Lomb-Scargle Periodogram Zonal 12h Amplitude Anomaly Trondheim

The Lomb-Scargle periodogram (Figure 5.5.2) indicates the presence of waves with larger than 16-days frequency at higher altitudes, with some 16-day wave presence

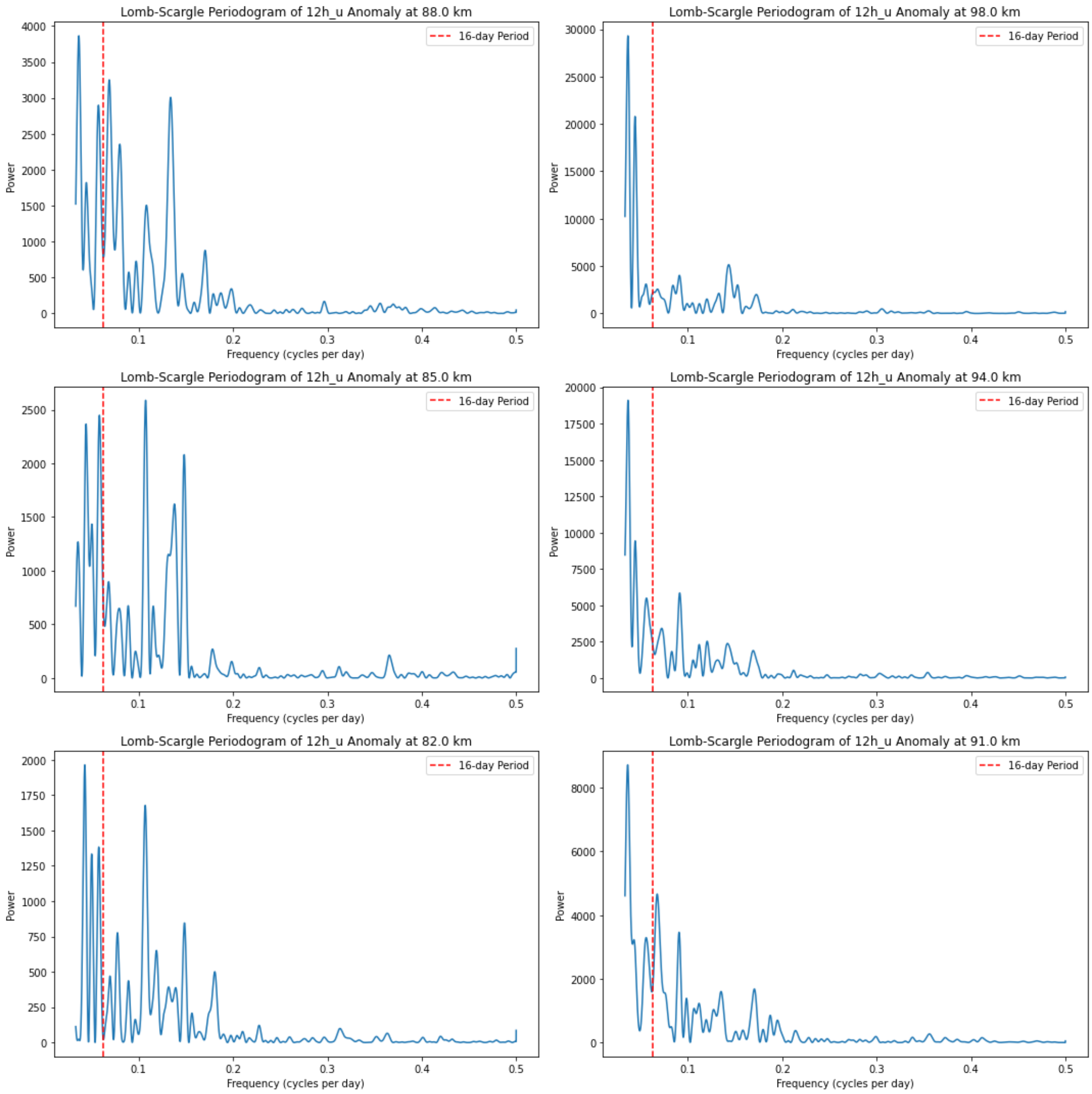

Figure 5.5.2: Lomb-Scargle periodogram for zonal 12h amplitude. The red line indicates the time of the eruption.

at lower altitudes.

5.5.3 Wavelet Zonal 12h Amplitude Anomaly Trondheim

The wavelet analysis (Figure 5.5.3) is impacted by bursts, complicating the identification of clear wave patterns. There might be waves of higher frequencies present, specially for the wavelet for 98km altitude, but there is not possible to know for sure, because of the bursts.

5.5.4 Meridional 12h Amplitude Trondheim

The climatology and anomaly plots for the meridional 12-hour amplitude are shown in Figure 5.5.4. As for the zonal 12h amplitude climatology, the meridional 12h amplitude climatology also have higher amplitudes at higher altitudes, which is also the case in the results from the study by Portnyagin et al. (1993)[31].

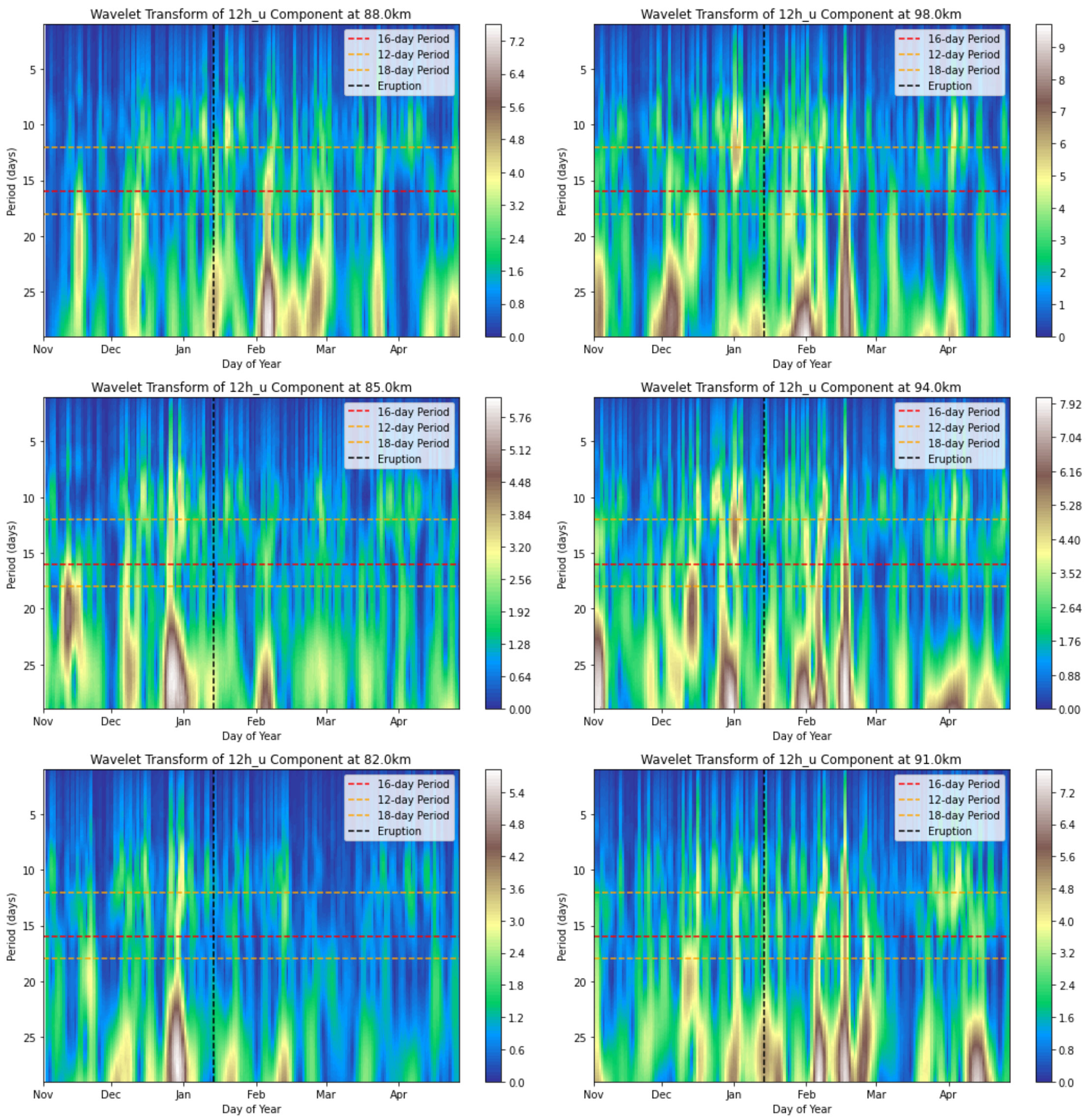

Figure 5.5.3: Wavelet 12h amplitude Trondheim. The red dashed line is the 16-day period, the orange lines are the 12- and 18-day period, while the black vertical dashed line is the eruption date.

The anomaly plot (5.5.4b) indicates the presence of waves longer than 16-days at higher altitudes, as for the zonal 12h amplitude results in Figure 5.5.1b.

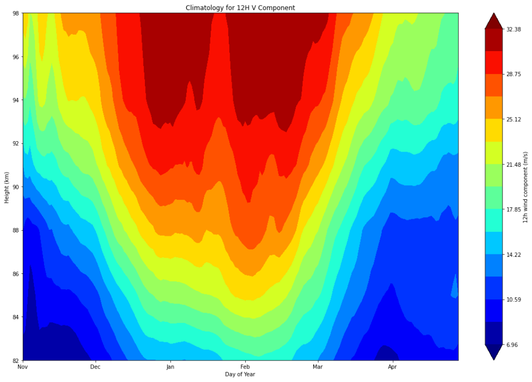

(a) Meridional climatology of the 12h amplitude in Trondheim

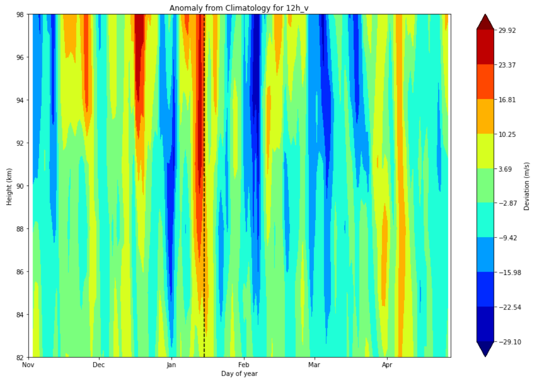

(b) Anomaly of the eruption period zonal 12h amplitude compared to the climatology

Figure 5.5.4: Meridional anomaly of the 12h amp in the eruption period compared to the climatology

5.5.5 Lomb-Scargle Periodogram Meridional 12h amplitude Trondheim

The Lomb-Scargle periodogram (Figure 5.5.5) confirms the presence of waves longer than 16-days at higher altitudes, with some 16-day wave presence at lower altitudes. There are noticeable similarities between the zonal and meridional results for the 12h amplitude.

5.5.6 Wavelet Zonal 12h Amplitude Anomaly Trondheim

The wavelet of the zonal 12h amplitude in Figure 5.5.6 is filled burst, similar as for the equivalent wavelets from the Rothera radar data. But there might be some presence of lower frequency waves around the 10 day mark. However, because there is multiple burst in the plot, another method would have to be used to make safe assumptions.

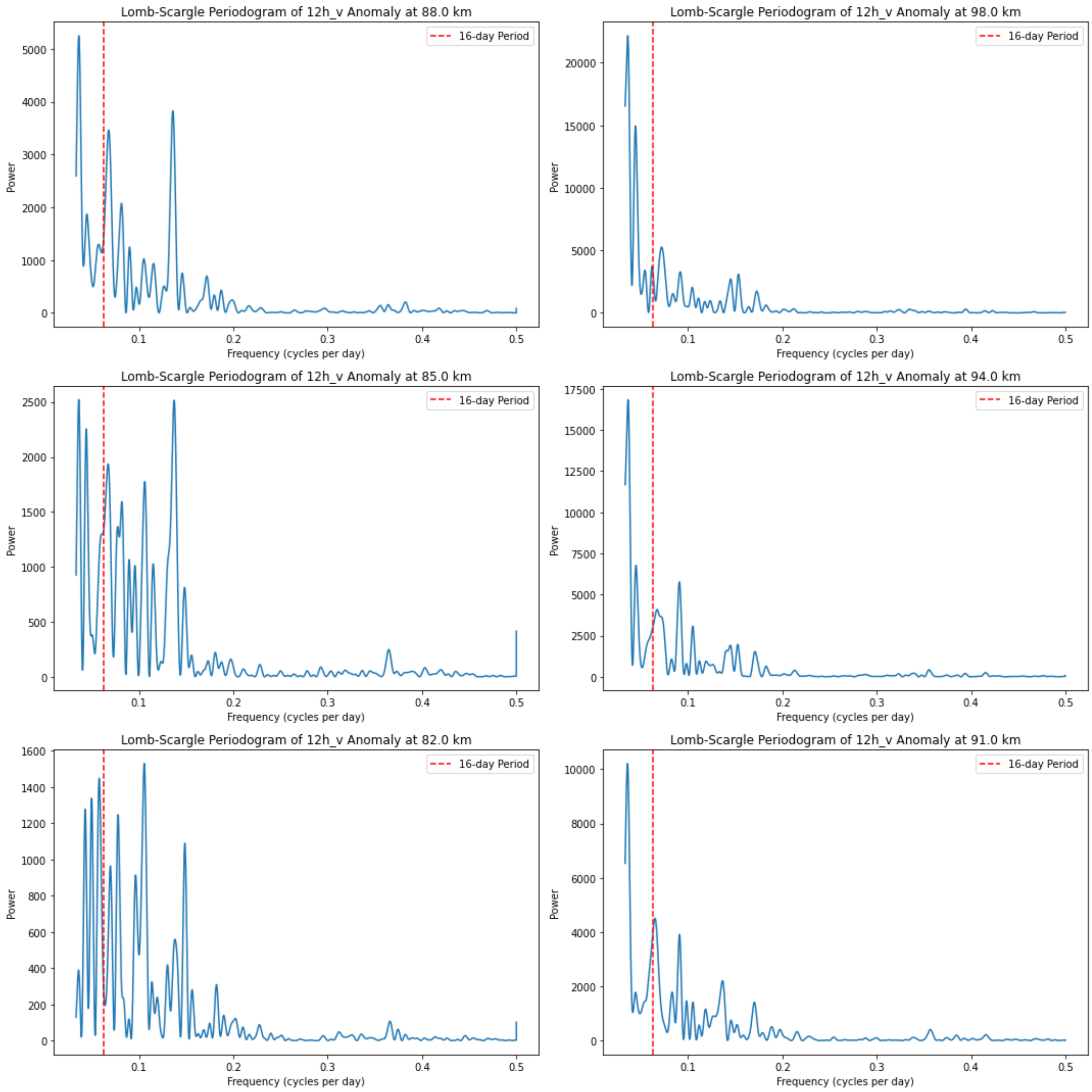

Figure 5.5.5: Meridional Lomb-Scargle 12h amplitude Trondheim

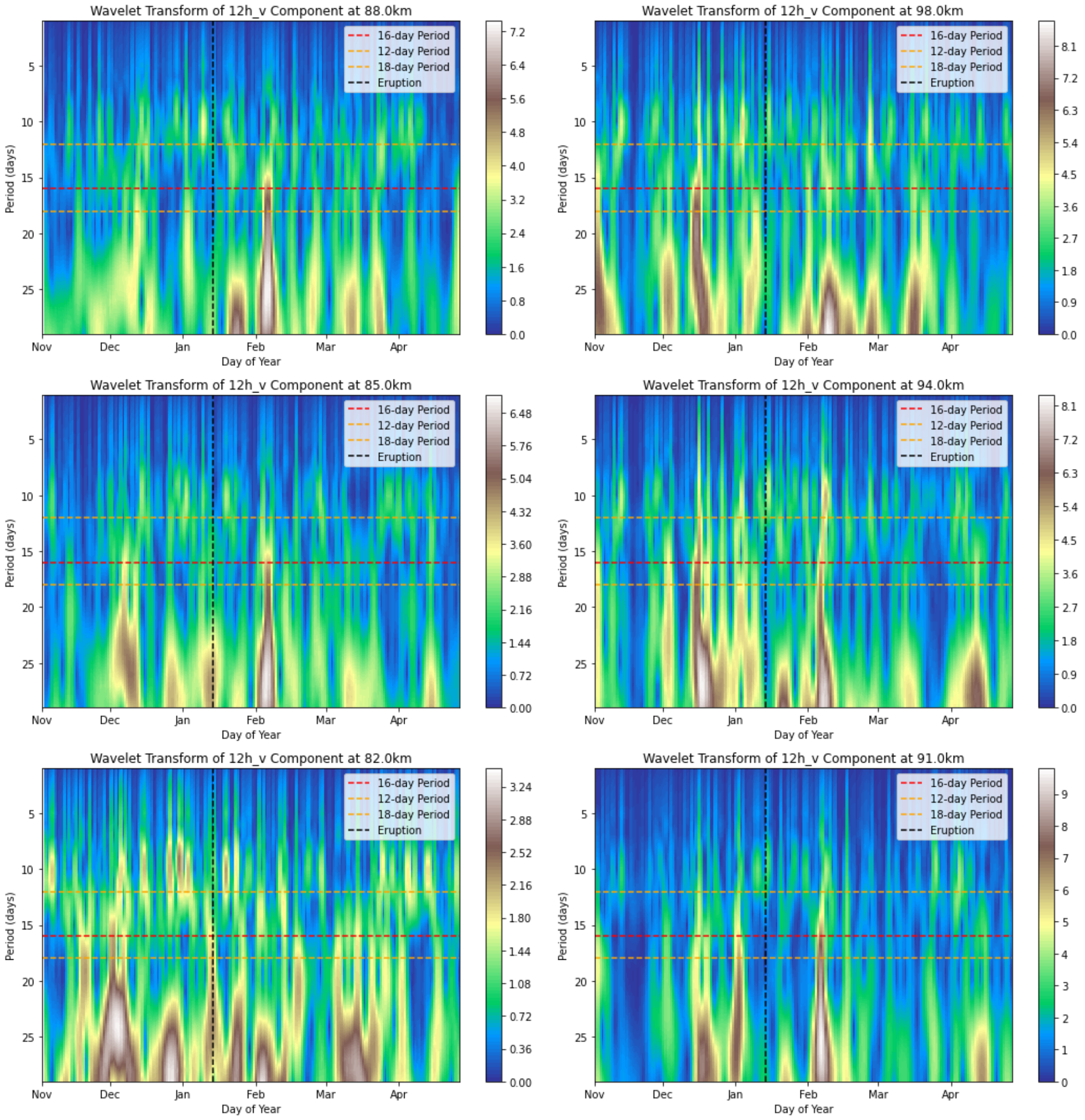

Figure 5.5.6: Wavelet meridional 12h amplitude Trondheim. The red dashed line is the 16-day period, the orange lines are the 12- and 18-day period, while the black vertical dashed line is the eruption date.

CHAPTER
SIX

CONCLUSIONS

This study has investigated the possibility that the Hunga Tonga-Hunga Ha'apai eruption influences the dynamics of the Mesosphere and Lower Thermosphere (MLT) using data from SKiYMET radars at Rothera and Trondheim. The analysis of anomalies in wind patterns and tidal amplitudes post-eruption did not conclusively determine whether the eruption affected atmospheric winds and the 16-day planetary wave. The presence of a 16-day wave, noted in both zonal and meridional wind components, suggests a potential influence, but the evidence is not definitive.

To draw more secure conclusions, further research is necessary. This includes examining the potential impact of the Sudden Stratospheric Warming (SSW) and Final Stratospheric Warming (SFW) by comparing the climatology to other periods beyond the eruption timeframe and analyzing differences. Such an approach will help isolate the effects of the eruption from other atmospheric phenomena. Future research directions should involve more extensive data analysis, including longer-term monitoring and other teqniques for analysing. These efforts would provide a deeper understanding of the long-term effects of volcanic eruptions on atmospheric dynamics.

Additionally, further studies could explore the interplay between different atmospheric layers and the propagation of tidal waves post-eruption. Investigating other volcanic events and comparing their impacts could also help establish a broader understanding of how such natural phenomena influence the MLT region.

As this study forms the basis for such efforts, it opens new avenues for exploration in atmospheric science and climatology. Enhancing our understanding of these dynamics will contribute to refining climatic models and improving predictions, ultimately aiding in better preparation for and response to atmospheric disturbances caused by volcanic eruptions and other significant events.

REFERENCES

[1] David G. Andrews. *An Introduction to Atmospheric Physics*. 2nd ed. Cambridge University Press, 2022.

[2] L. Coy et al. “Stratospheric circulation changes associated with the Hunga Tonga-Hunga Ha’apai eruption”. In: *Geophysical Research Letters* 49.e2022GL100982 (2022). DOI: 10.1029/2022GL100982.

[3] Corwin J. Wright et al. “Hunga Tonga-Hunga Ha’apai eruption”. In: *Nature* (). DOI: 10.1038/s41586-022-05012-5.

[4] R. E. Hibbins, P. J. Espy, and M. J. Jarvis. “Mean winds and tides in the mesosphere and lower thermosphere above Halley, Antarctica”. In: *Journal of Atmospheric and Solar-Terrestrial Physics* 68.4 (), pp. 436–444.

[5] Ucar Center for Science Education. *Layers of Earth’s Atmosphere | Center for Science Education*. [Online; accessed 21. Nov. 2023]. Nov. 2023. URL: https://scied.ucar.edu/learning-zone/atmosphere/layers-earths-atmosphere.

[6] Unknown Author. *Derivation of Trace Gas Information combining Differential Optical Absorption Spectroscopy with Radiative Transfer Modelling*. Scientific Figure on ResearchGate. Available from: https://www.researchgate.net/figure/1-Vertical-structure-of-the-earth-s-atmosphere-The-temperature-profile-is-an-idealized_fig1_33427973. Accessed: 2023. URL: https://www.researchgate.net/figure/1-Vertical-structure-of-the-earth-s-atmosphere-The-temperature-profile-is-an-idealized_fig1_33427973.

[7] Robert A. Vincent. “The dynamics of the mesosphere and lower thermosphere: a brief review”. In: *Prog. Earth Planet. Sci.* 2.1 (Dec. 2015), pp. 1–13. ISSN: 2197-4284. DOI: 10.1000/exampledoi.

[8] Jeffrey M. Forbes. “Vertical Coupling by the Semidiurnal Tide in Earth’s Atmosphere”. In: *Climate and Weather of the Sun-Earth System (CAWSES)*. 2009.

[9] Kjetil Landgraff Ekern. “Climatology of Short-Period Tidal Oscillations in the Upper Atmosphere”. Master’s thesis. NTNU, 2013.

[10] C. Donald Ahrens. *Meteorology Today: An Introduction to Weather, Climate, and the Environment*. Cengage Learning, 2012.

[11] W. R. Peltier. “On the hemispheric origins of meltwater pulse 1a”. In: *Quaternary Science Reviews* (2005).

[12] Feng He et al. “Northern Hemisphere forcing of Southern Hemisphere climate during the last deglaciation”. In: *Nature* (2013).

[13] Shaun M. Dempsey et al. “Winds and tides of the Antarctic mesosphere and lower thermosphere: One year of meteor-radar observations over Rothera (68◦S, 68◦W) and comparisons with WACCM and eCMAM”. In: *Journal of Atmospheric and Solar-Terrestrial Physics* 212 (2021), p. 105510. DOI: 10.1016/j.jastp.2020.105510. URL: https://doi.org/10.1016/j.jastp.2020.105510.

[14] W.K. Hocking, B. Fuller, and B. Vandepeer. “Real-time determination of meteor-related parameters utilizing modern digital technology”. In: *Journal of Atmospheric and Solar-Terrestrial Physics* 63 (2001), pp. 155–169.

[15] N.H. Kolnes. *Doppler Imaging Of Gravity Waves*. Specialization Project. 2012.

[16] *Atmospheric Group Webpage*. Accessed: 2023-December. URL: https://home.phys.ntnu.no/brukdef/prosjekter/atmosfys/web-pages/SKiYMET-wind.php.

[17] R. E. Hibbins and M. J. Jarvis. “A long-term comparison of wind and tide measurements in the upper mesosphere recorded with an imaging Doppler interferometer and SuperDARN radar at Halley, Antarctica”. In: *Atmospheric Chemistry and Physics* 8.5 (2008), pp. 1367–1376. DOI: 10.5194/acp-8-1367-2008. URL: https://acp.copernicus.org/articles/8/1367/2008/.

[18] Christophe Leys et al. “Detecting outliers: Do not use standard deviation around the mean, use absolute deviation around the median”. In: *Journal of Experimental Social Psychology* 49.4 (2013), pp. 764–766.

[19] *DEALING WITH MEASUREMENT NOISE - Averaging Filter*. [Online; accessed 12. Jun. 2024]. June 2024. URL: https://web.archive.org/web/20100329134203/http://lorien.ncl.ac.uk/ming/filter/filmav.htm.

[20] Jacob T. VanderPlas. “Understanding the Lomb–Scargle Periodogram”. In: *The Astrophysical Journal Supplement Series* 236.1 (May 2018), p. 16. DOI: 10.3847/1538-4365/aab766. URL: https://dx.doi.org/10.3847/1538-4365/aab766.

[21] Christopher Torrence and Gilbert P. Compo. “A Practical Guide to Wavelet Analysis”. In: *Bulletin of the American Meteorological Society* 79.1 (1998), pp. 61–78. DOI: 10.1175/1520-0477(1998)079<0061:APGTWA>2.0.CO;2. URL: https://doi.org/10.1175/1520-0477(1998)079%3C0061:APGTWA%3E2.0.CO;2.

[22] R. E. Hibbins et al. “Seasonal variations in the horizontal wind structure from 0-100 km above Rothera station, Antarctica (67° S, 68° W)”. In: *Atmospheric Chemistry and Physics* 5.11 (2005), pp. 2973–2980.

[23] Fan Rong Yu et al. “Quasi 10-and 16-Day Wave Activities Observed Through Meteor Radar and MST Radar During Stratospheric Final Warming in 2015 Spring”. In: *Journal of Geophysical Research: Atmospheres* 124.12 (2019), pp. 6040–6056. DOI: 10.1029/2019JD030630.

[24] Jincai Xie et al. "The onset of stratospheric final warming and record–breaking April surface warming over Central Asia in 2022". In: *Dynamics of Atmospheres and Oceans* 103 (2023), p. 101373. ISSN: 0377-0265. DOI: https://doi.org/10.1016/j.dynatmoce.2023.101373. URL: https://www.sciencedirect.com/science/article/pii/S0377026523000246.

[25] J.M. Forbes et al. "Quasi 16-day oscillation in the mesosphere and lower thermosphere". In: *Journal of Geophysical Research: Atmospheres* 100.D5 (1995), pp. 9149–9163.

[26] N. H. Stray et al. "Observations of planetary waves in the mesosphere-lower thermosphere during stratospheric warming events". In: *Atmospheric Chemistry and Physics* 15.9 (2015). © Author(s) 2015. CC Attribution 3.0 License., pp. 4997–5005. DOI: 10.5194/acp-15-4997-2015. URL: https://www.atmos-chem-phys.net/15/4997/2015/.

[27] P. Kishore et al. "Impact of Stratospheric Sudden Warming on the Tropopause, Stratopause and Mesopause". In: *Remote Sensing of Environment* 184 (2016), pp. 263–275. DOI: 10.1016/j.rse.2016.07.008. URL: https://doi.org/10.1016/j.rse.2016.07.008.

[28] R.E. Hibbins et al. "A climatology of tides and gravity wave variance in the MLT above Rothera, Antarctica obtained by MF radar". In: *Journal of Atmospheric and Solar-Terrestrial Physics* 69 (2007), pp. 578–588. DOI: 10.1016/j.jastp.2006.10.009.

[29] R. Stockwell. "Why use the S-Transform?" In: *American Mathematical Society Pseudo-differential equations and time frequency analysis* 52 (Jan. 2007).

[30] D. J. Sandford et al. "Dynamics of the Antarctic and Arctic mesosphere and lower thermosphere – Part 1: Mean winds". In: *Atmospheric Chemistry and Physics* 10 (2010), pp. 10273–10289. DOI: 10.5194/acp-10-10273-2010. URL: https://www.atmos-chem-phys.net/10/10273/2010/.

[31] Yu. I. Portnyagin et al. "Dynamics of the Antarctic and Arctic mesosphere and lower thermosphere regions-II. The semidiurnal tide". In: *Journal of Atmospheric and Terrestrial Physics* 55.6 (1993), pp. 843–855.

APPENDICES

A - EXTRACTED 16-DAY WAVES

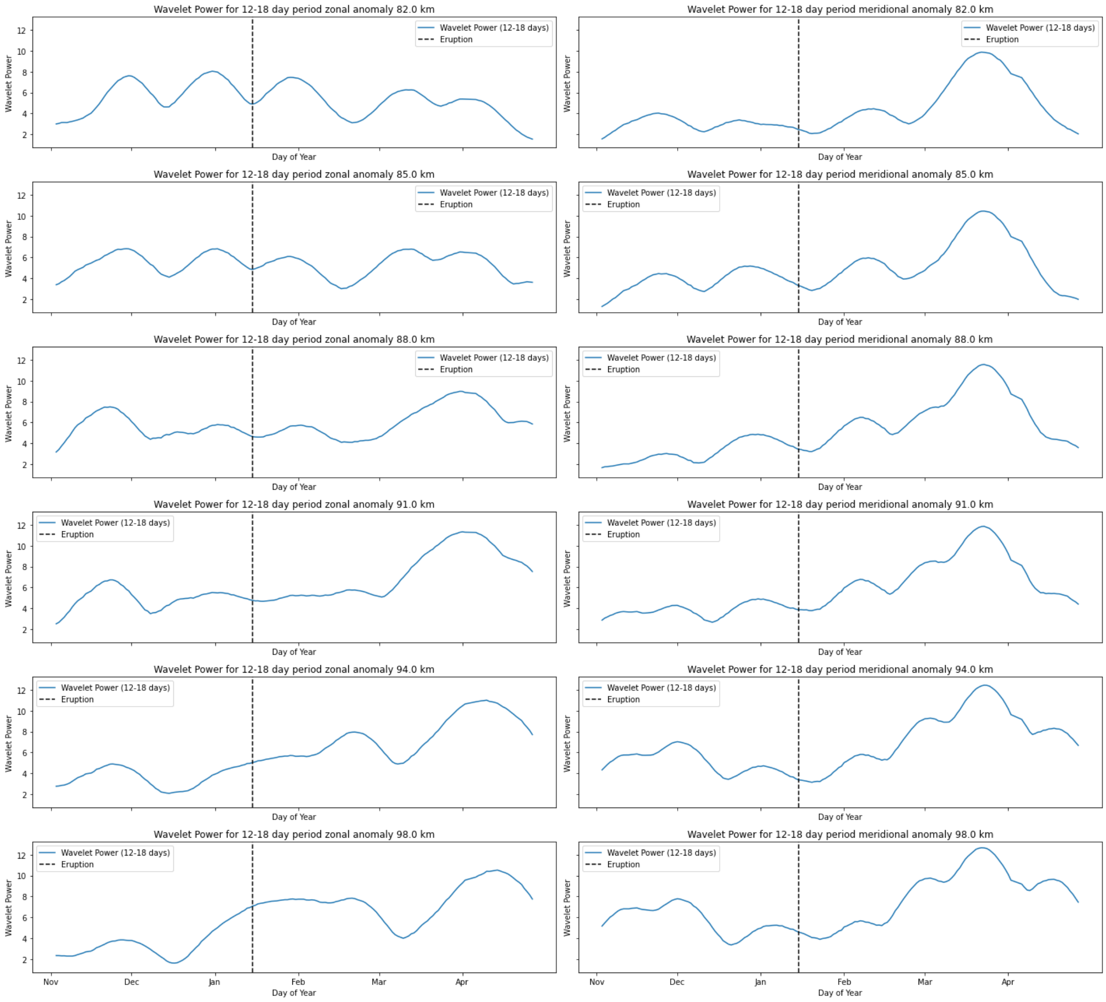

Figure .0.1: Extracted 16-day (using 12-18 days) wave for the Rothera mean wind anomalies.

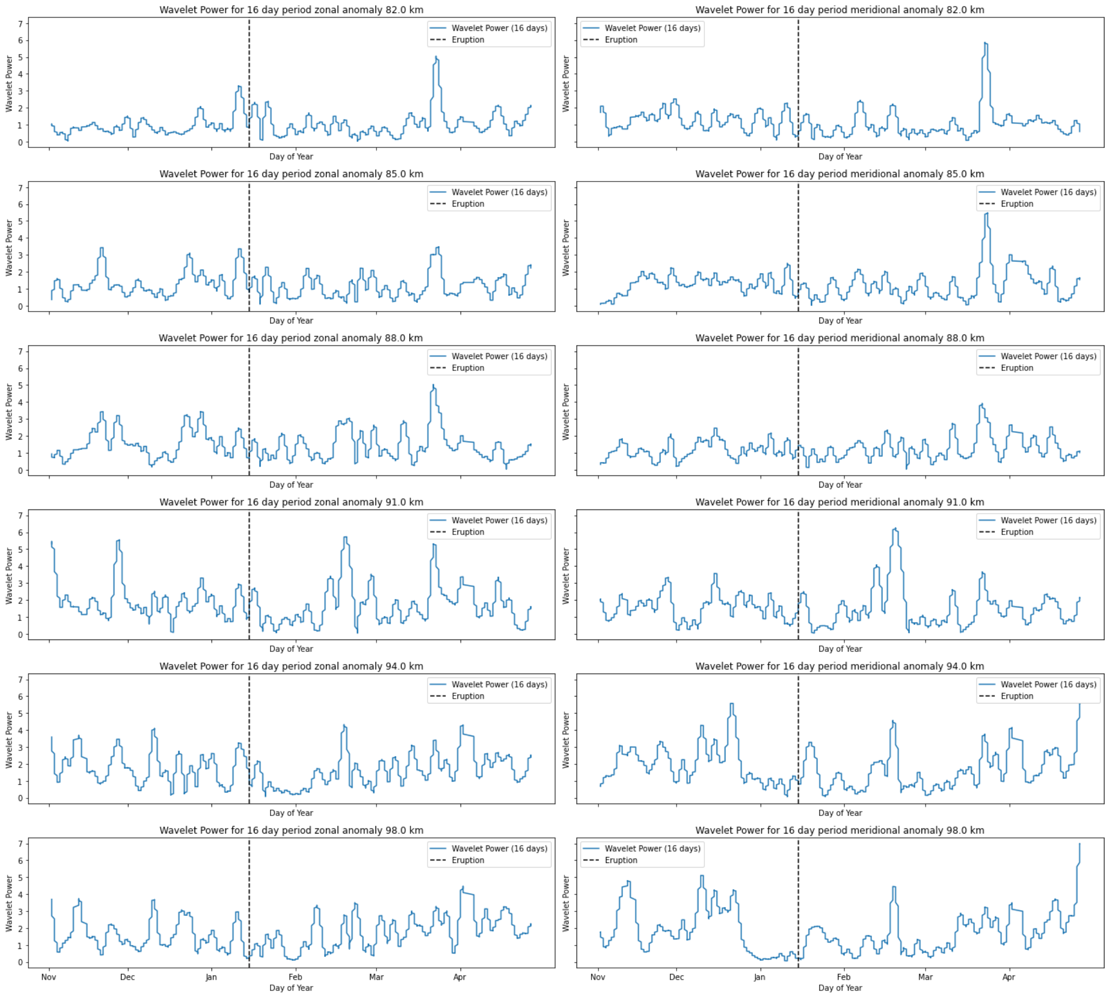

Figure .0.2: Extracted 16-day (using 12-18 days) wave for the Rothera 12h amplitude anomalies.

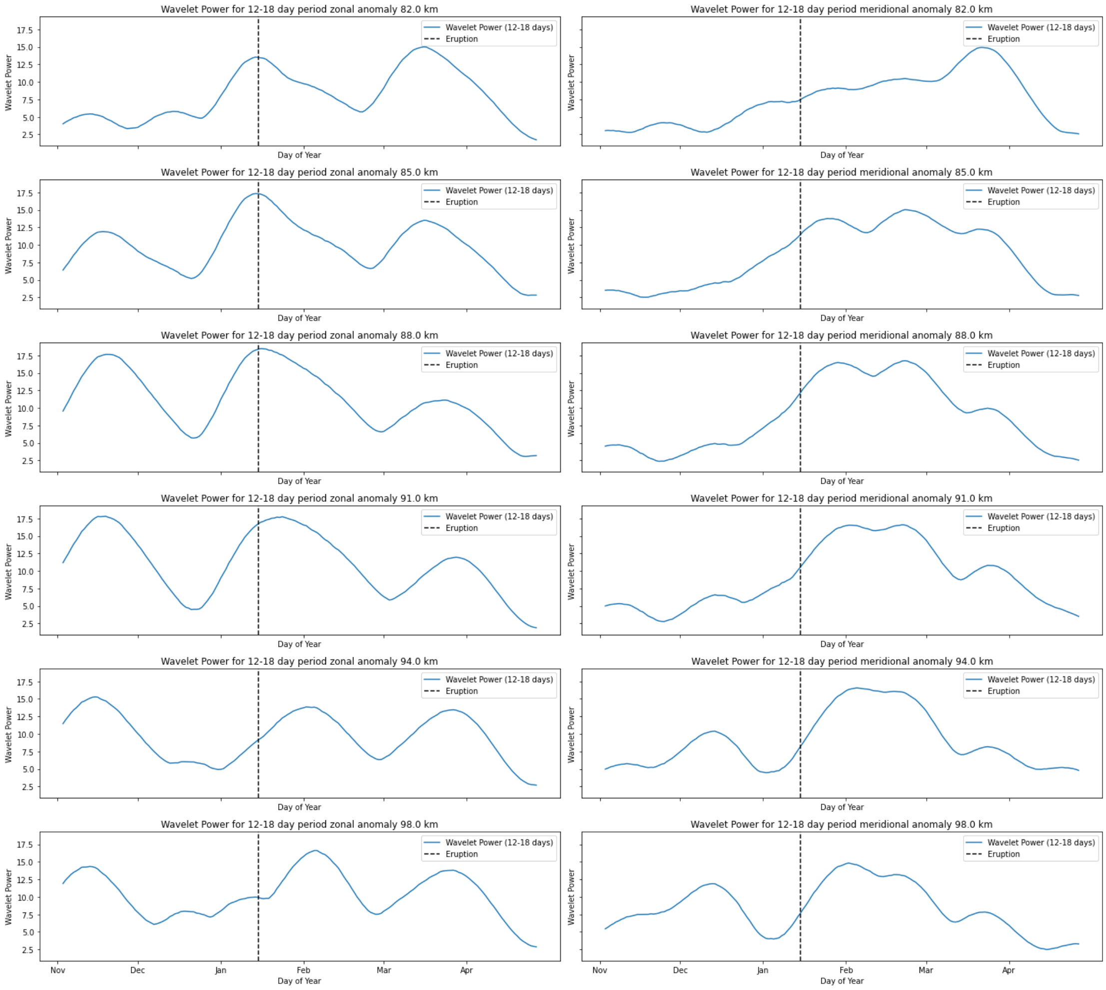

Figure .0.3: Extracted 16-day (using 12-18 days) wave for the Trondheim mean wind anomalies.

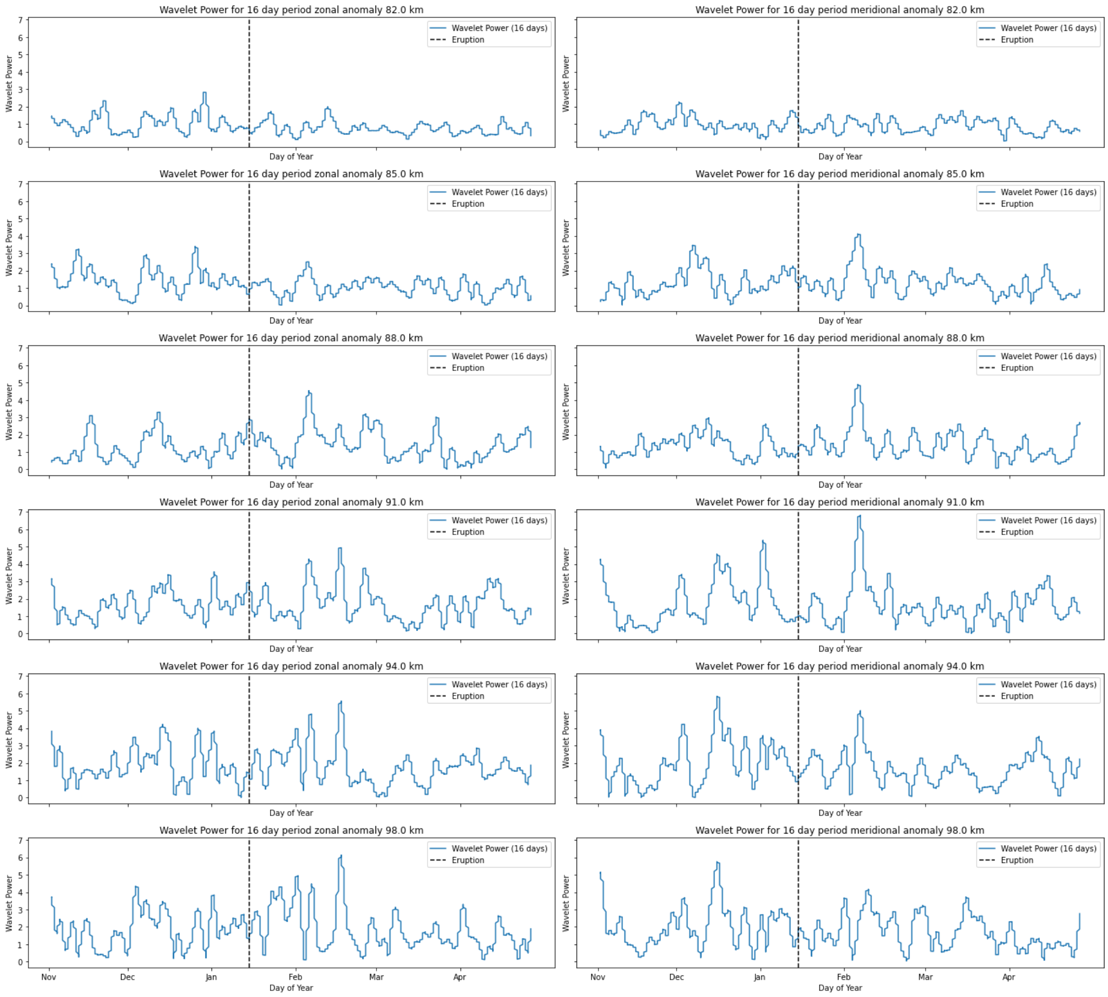

Figure .0.4: Extracted 16-day (using 12-18 days) wave for the Trondheim 12h amplitude anomalies

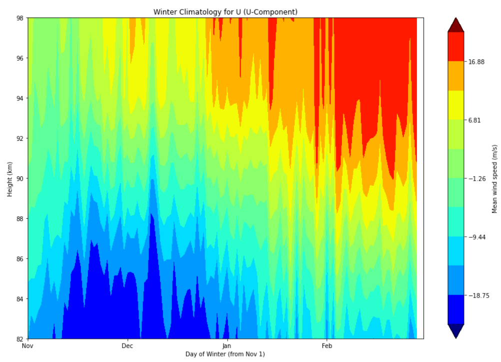

(a) Zonal Raw Wind Climatology

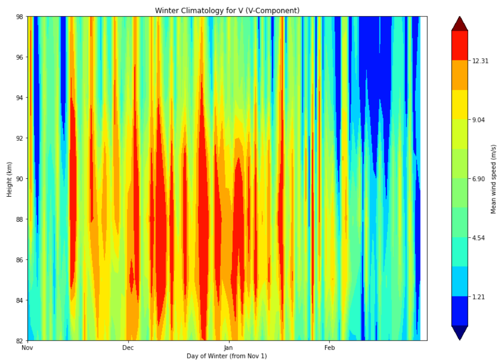

(b) Meridional Raw Wind Climatology

Figure .0.5: Raw climatology Rothera

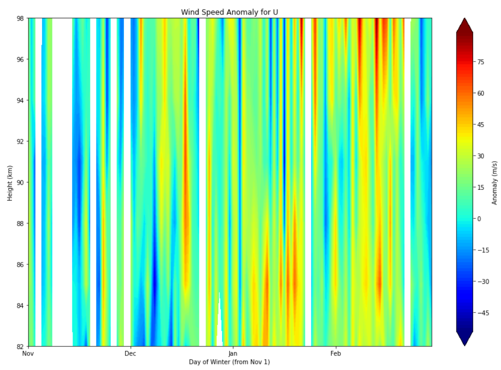

(a) Zonal Raw Wind Anomaly Rothera

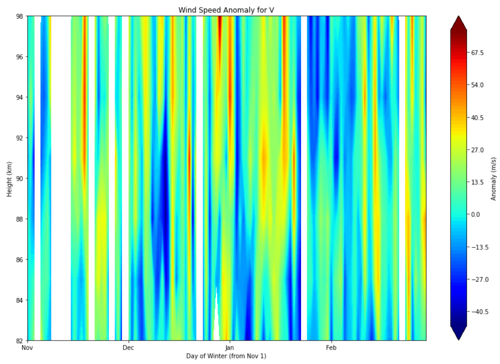

(b) Meridional Raw Wind Anomaly Rothera

Figure .0.6: Raw Anomaly Plots Rothera

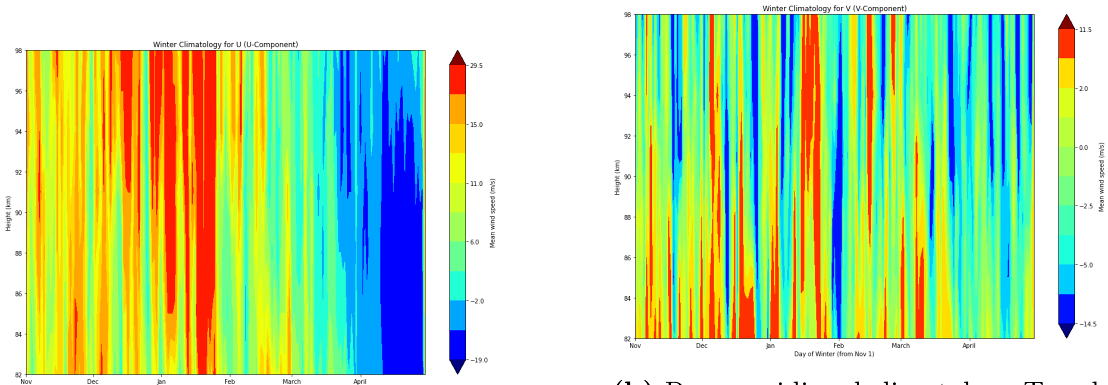

(a) Raw zonal climatology Trondheim

(b) Raw meridional climatology Trondheim

Figure .0.7: Raw climatologies Trondheim

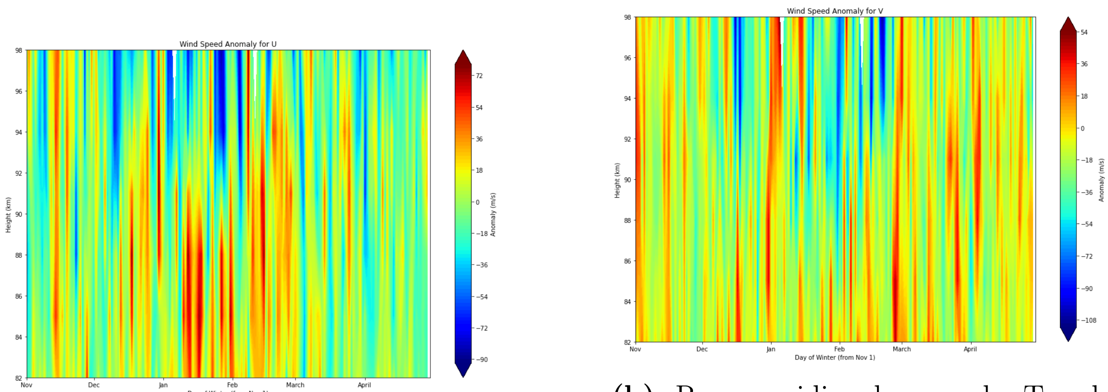

(a) Raw zonal anomaly Trondheim

(b) Raw meridional anomaly Trondheim

Figure .0.8: Raw anomaly plots Trondheim

C - LOMB-SCARGLE PERIODOGRAM RAW DATA TRONDHEIM

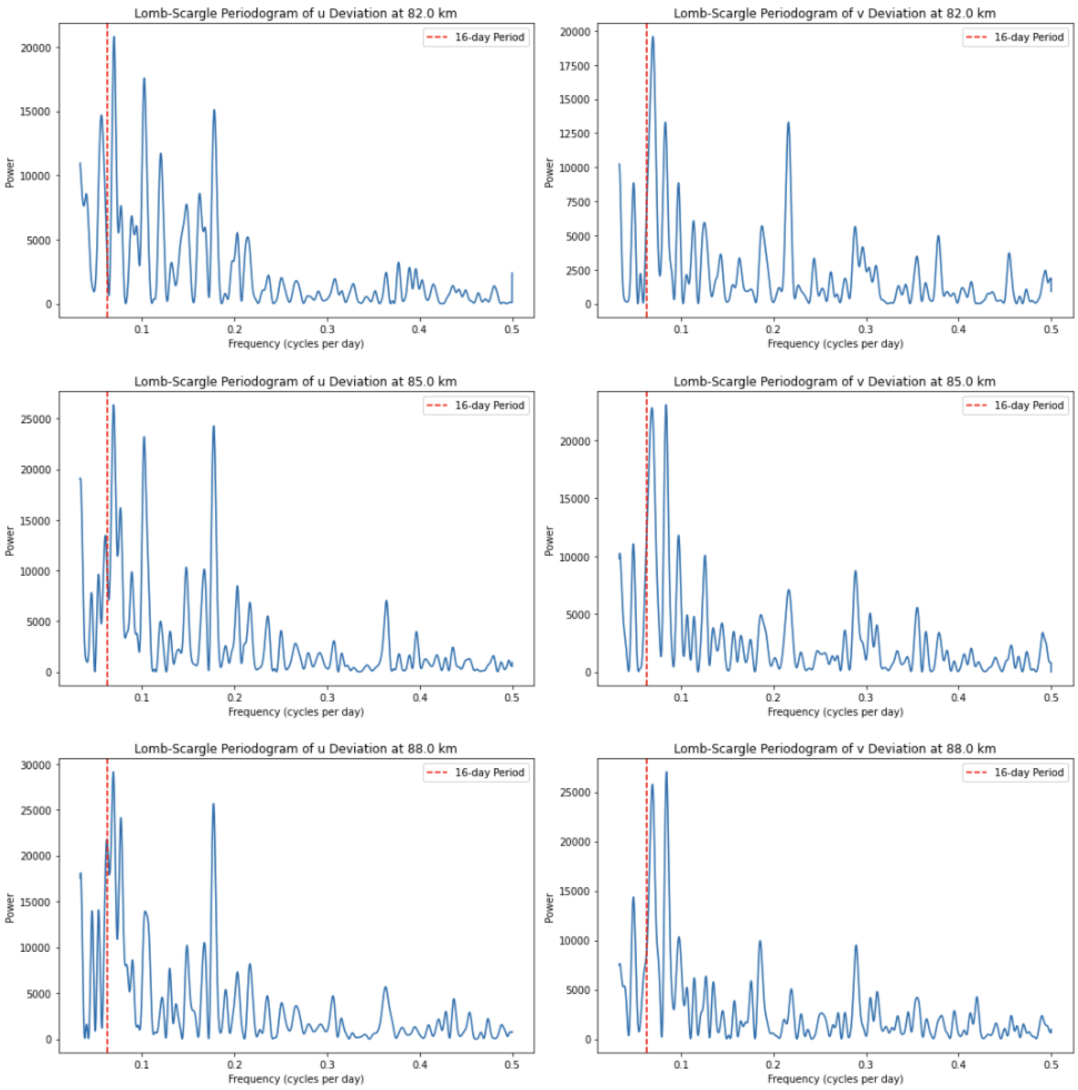

Figure .0.9: Lomb-Scargle Periodogram of raw wind data from Trondheim at 82km, 85km and 88km for both zonal and meridional winds

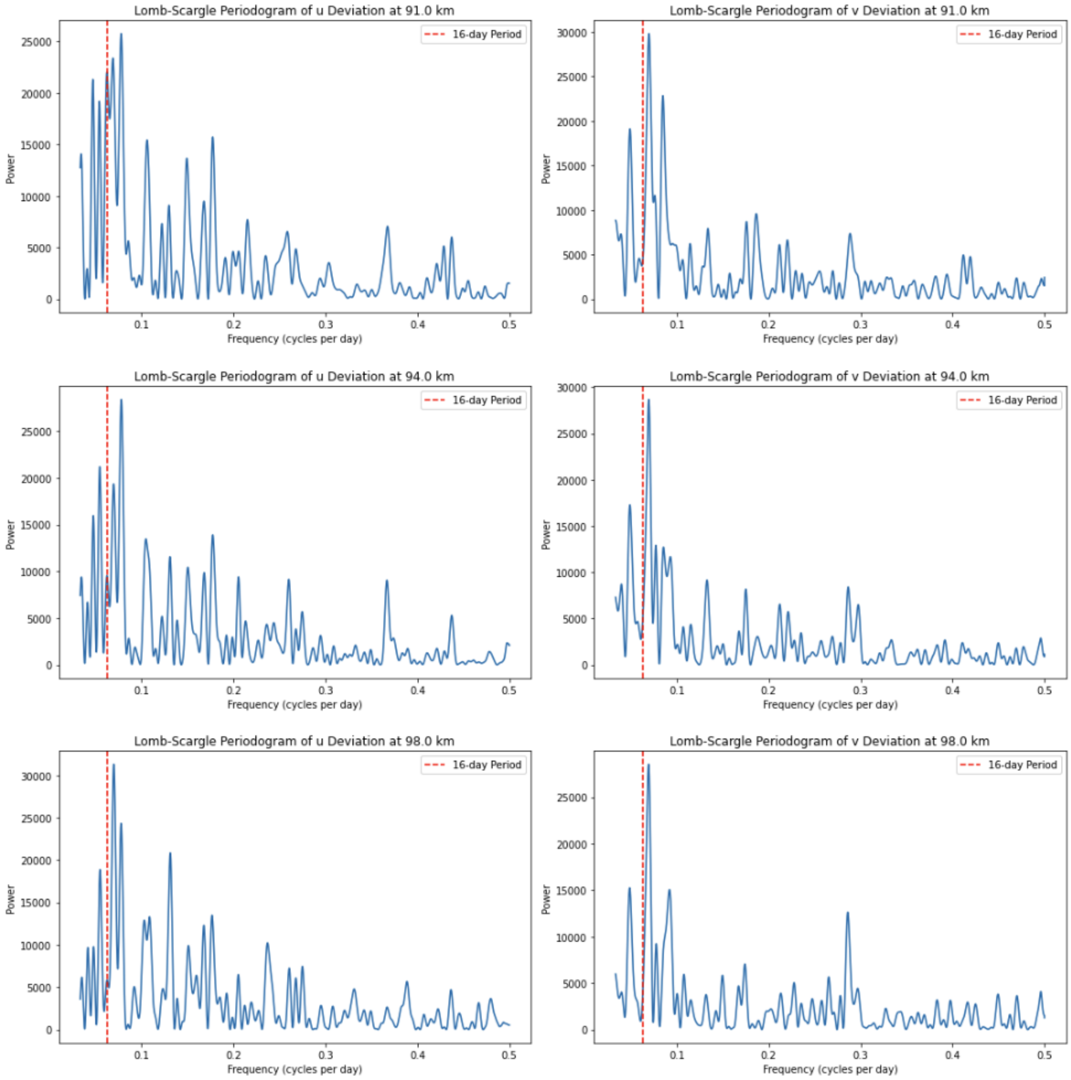

Figure .0.10: Lomb-Scargle Periodogram of raw wind data from Trondheim at 91km, 94km and 98km for both zonal and meridional winds

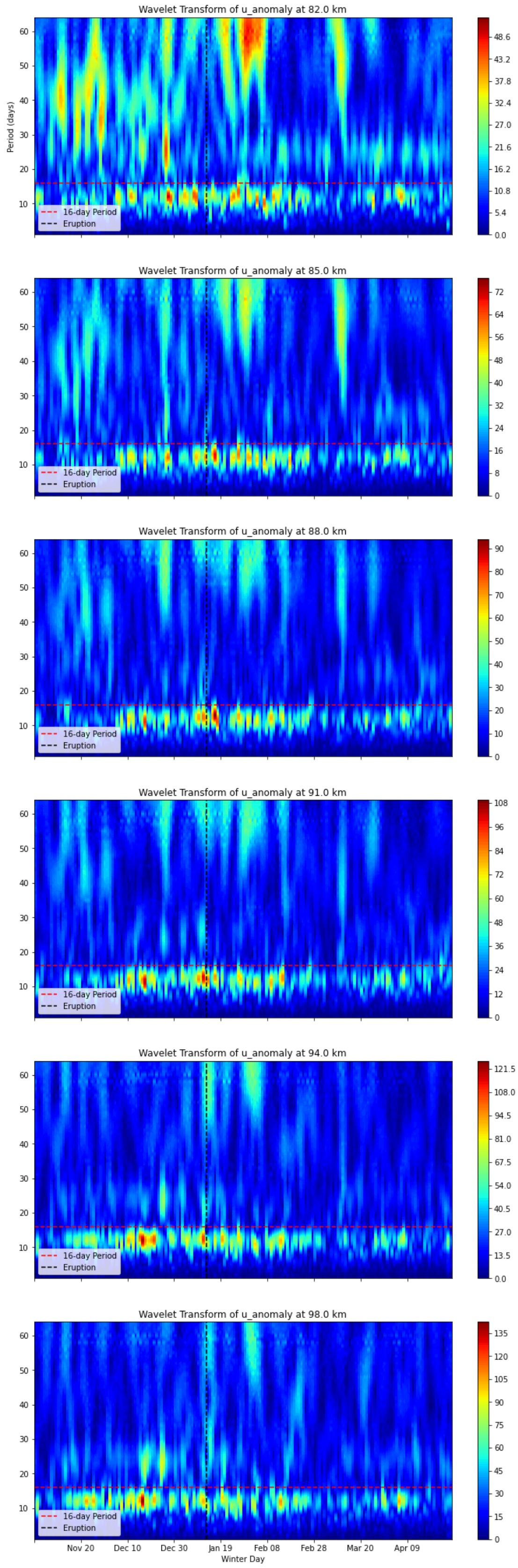

Figure .0.11: Wavelets of raw zonal data Trondheim

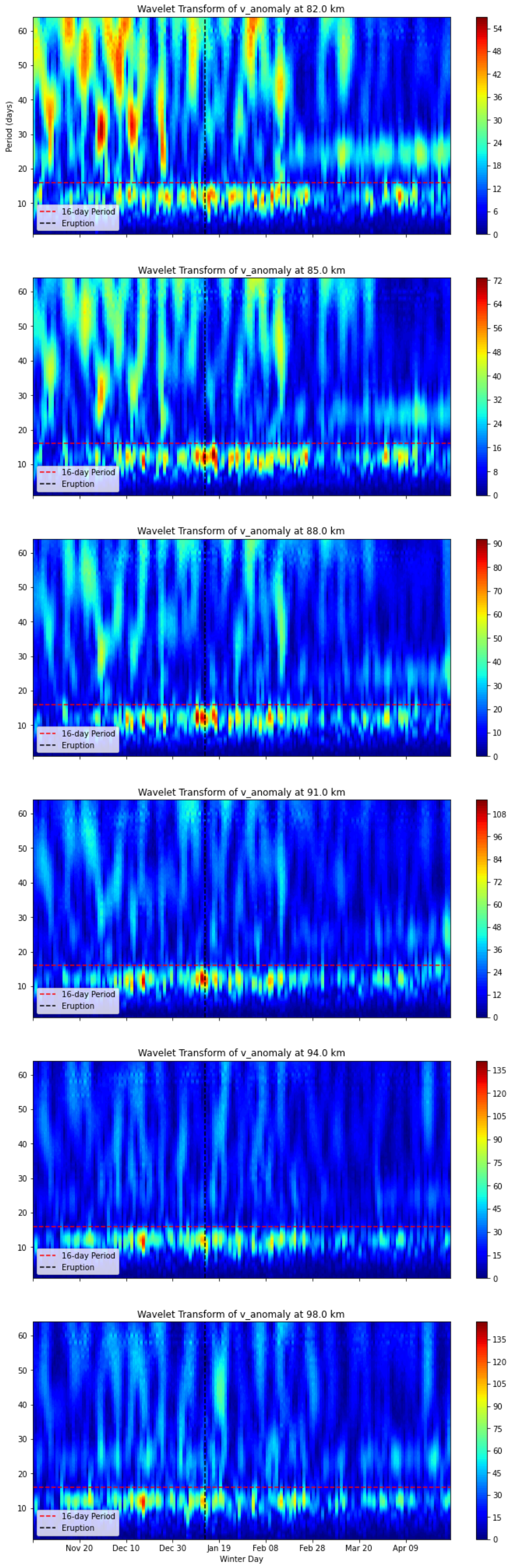

Figure .0.12: Wavelets of raw meridional data Trondheim

NTNU

Norwegian University of
Science and Technology